Structural control on fluid flow and shallow diagenesis: Insights from calcite cementation along deformation bands in porous sandstones

Leonardo DEL SOLE[1], Marco ANTONELLINI[1], Roger SOLIVA[2], Gregory BALLAS[2], Fabrizio BALSAMO[3], and Giulio VIOLA[1]

[1]BiGeA - Department of Biological, Geological and Environmental Sciences, University of Bologna, Via Zamboni 67, 40126 Bologna, Italy

[2]Laboratoire Géosciences Montpellier, Université de Montpellier, CNRS, Université des Antilles, Montpellier, France.

[3]Next, Natural and Experimental Tectonic Research Group, Department of Chemistry, Life, Sciences and Environmental Sustainability, University of Parma, Parco Area delle Scienze 157A, 43124 Parma, Italy

Correspondence: Leonardo Del Sole (leonardo.delsole@unibo.it)

Abstract. Porous sandstones are important reservoirs for geofluids. Interaction therein between deformation and cementation during diagenesis is critical since both processes can strongly reduce rock porosity and permeability, deteriorating reservoir quality. Deformation bands (DBs) and structural-related diagenetic bodies, here named Structural and Diagenetic Heterogeneities (SDH), affect fluid flow at a range of scales and potentially lead to reservoir compartmentalization, influencing flow buffering and sealing during production of geofluids. We present two field-based studies from Loiano (Northern Apennines, Italy) and Bollène (Provence, France) that elucidate the structural control exerted by DBs on fluid flow and diagenesis recorded by calcite nodules associated with the bands. We relied on careful *in situ* observations through geo-photography, string mapping, and UAV aerial photography, integrated with optical, scanning electron and cathodoluminescence microscopy, and stable isotope ($\delta^{13}C$ and $\delta^{18}O$) analysis of nodules cement. In both case studies, one or more sets of DBs precede and control selective cement precipitation. Cement texture and cathodoluminescence patterns, and their invariably negative $\delta^{13}C$ and $\delta^{18}O$ value ranges, suggest a meteoric environment for nodule formation. In Loiano, DBs acted as low-permeability barriers to fluid flow and promoted selective cement precipitation. In Bollène, clusters of DBs restricted fluid flow and focused diagenesis in parallel-to-band compartments. Our work shows that DBs control flow pattern within a porous sandstone reservoir and this, in turn, affects how diagenetic heterogeneities are distributed within the porous rocks. This information is invaluable to assess the uncertainties in reservoir petrophysical properties especially where SDH are below seismic resolution. The localization of cement along DBs further enhance the flow buffering potential of these structural features.

1 Introduction

Porous rocks, such as sandstones and carbonates, are important reservoirs for geofluids. Structural and diagenetic processes commonly affect the petrophysical properties and reservoir quality in these rocks. The importance of the interaction between deformation and deformational structures, fluid flow, and diagenetic processes has been emphasized only during the last two decades (e.g. see the recently coined term "*structural diagenesis"*, Laubach et al., 2010; Mozley and Goodwin, 1995; Eichhubl et al., 2009; Balsamo et al., 2012; Philit et al., 2015; Antonellini et al., 2017, 2020; Del Sole et al., 2020). If deformation influences diagenesis and vice-versa, a feedback can eventually develop between these two processes. Early diagenesis influences the mechanical properties of rocks (Antonellini et al., 2020), and, in turn, their mechanical stratigraphy (Laubach et al., 2009; La Bruna et al., 2020). Structural and diagenetic heterogeneities (referred to as SDH from now on) can determine the texture as well as the petrophysical and mechanical properties of the rock volume hosting them (Antonellini and Aydin, 1994; Aydin, 2000; Faulkner et al., 2010; Bense et al., 2013; Pei et al., 2015; Del Sole et al., 2020). Cement precipitation in granular porous siliciclastic rocks leads to porosity loss and reduction in permeability (Tenthorey et al., 1998; Morad et al., 2010) and, in turn, overall reservoir quality deterioration (Ehrenberg, 1990; Morad et al., 2010). Carbonate cement is commonly concentrated within a few, specific horizons or nodules with various shapes and arrangements (Kantorowicz et al., 1987; Bjørkum and Walderhaug, 1990; Mozley and Davis, 1996) making porosity and permeability prediction more complex (Davis et al., 2006; Morad et al., 2010). Furthermore, cement increases the mechanical strength of the host rock (Dvorkin et al., 1991; Bernabé et al., 1992, Boutt et al., 2014) influencing fault-zone architecture and potential fault reactivation (Dewhurst and Jones, 2003; Flodin et al., 2003; Wilson et al., 2006; Williams et al., 2017; Philit et al., 2019; Pizzati et al., 2019).

Granular or porous sediments and sedimentary rocks commonly contain sub-seismic resolution strain localization features referred to as deformation bands (Aydin, 1978; DBs from now on). The effect of DBs on fluid flow can significantly vary. Their overall different behavior depends on several factors, such as their permeability contrast relative to the host rock, their thickness, density, distribution, orientation, segmentation, and connectivity (Antonellini and Aydin, 1994; Gibson, 1998; Manzocchi et al., 1998; Sternlof et al., 2004; Shipton et al., 2005; Fossen and Bale, 2007; Torabi and Fossen 2009; Rotevatn et al., 2013; Soliva et al., 2016). In some cases, DBs appear to be conduits for fluids (Parry et al. 2004; Sample et al. 2006; Petrie et al., 2014; Busch et al., 2017). In most of cases, however, they are associated with a strong porosity and permeability reduction relative to the host rock (Antonellini and Aydin, 1994; Fisher and Knipe, 2001; Shipton et al., 2002; Sternlof et al., 2004; Balsamo and Storti, 2010; Ballas et al., 2015; Fossen et al., 2017; Del Sole and Antonellini, 2019) inducing permeability anisotropy and reservoir compartmentalization. This might impact negatively upon production from faulted siliciclastic systems (Edwards et al., 1993; Lewis and Couples, 1993; Leveille et al., 1997; Antonellini et al., 1999; Wilkins et al., 2019) and flow-based models and simulations (Sternlof et al. 2004; Rotevatn and Fossen, 2011; Fachri et al., 2013; Qu and Tveranger, 2016; Romano et al., 2020).

Cements have been found in association with DBs. Localization of cement along these structural features may significantly enhance porosity and permeability reduction caused by mechanical crushing and reorganization of grains, thus increasing their sealing or buffering potential (Edwards et al., 1993; Leveille et al., 1997; Fisher and Knipe, 1998; Parnell et al., 2004; Del Sole et al., 2020). Therefore, occurrence, distribution, and petrophysical properties of cement along DBs need to be properly characterized and implemented into reservoir quality models to predict porosity and permeability, and their heterogeneity (e.g. Morad et al., 2010).

Models for calcite cementation, besides, are fundamental for predicting sandstone and fault-rock properties such as porosity, permeability, compressibility, and seismic attributes. Diagenetic processes related to fluid-flow mechanisms and evolution within DBs remain poorly constrained. Different processes account for enhanced fluid flow within DBs, such as unsaturated flow relative to the host rock in arid to semiarid vadose zones, (Sigda et al., 1999; Sigda and Wilson, 2003); and transient dilation in the early stage of DB formation (e.g. Antonellini et al., 1994; Main et al., 2000). As well, these mechanisms have been employed to explain the occurrence of cement and other processes (e.g. cementation, hydrocarbon inclusion entrapment, removal of iron oxide coatings) in and around the band (Fowles and Burley, 1994; Labaume and Moretti, 2001; Ogilvie and Glover, 2001; Parnell et al., 2004; Parry et al., 2004; Sample et al., 2006; Wilson et al., 2006; Cavailhes et al., 2009; Balsamo et al., 2012; Lommatzsch et al., 2015). These mechanisms, however, appear to be limited to specific conditions (e.g. cement precipitation in the early stage of DB formation, or in vadose environments) and they assume that DBs behaved as fluid "conduits" in order to explain the occurrence of cement or other authigenic products within these structures. Nevertheless, a significant number of studies on DBs show that in most cases they are baffle or seals to fluid flow (see Ballas et al., 2015 for a review). Much less work has been addressed to elucidate the fluid flow and diagenetic mechanisms leading to selective cementation in association with low-permeability baffle/barrier DBs (Philit et al., 2015; Williams et al., 2015). Different mechanisms, then, need to be invoked to explain the occurrence of cement in association with DBs in a broader set of conditions.

The aim of our work is to elucidate the hydraulic behavior of DBs as well as fluid flow mechanisms and evolution, with regards to diagenetic processes, related to such structures. The novelty of our work is that by using a cross-disciplinary study integrating structural and diagenetic analysis, we constrain the interaction between DBs, fluid flow, and diagenesis. In particular, we assess the control exerted by DBs on flow pattern and diagenetic heterogeneities distribution, by characterizing the occurrence, and the spatial and microstructural relationship between DBs and cement nodules in two porous sandstone reservoir analogs. We examine two field sites in Italy and France where calcite cement nodules are spatially associated with DBs. The comparison between the two locations with different geological settings makes it possible to derive general conclusions that can be extended to other cases where DBs and diagenetic processes interact. Our study allows also to evaluate the impact of both structural and structural-related diagenetic heterogeneities on present-time fluid circulation and on subsequent deformation.

2 Geological framework

2.1 Loiano field site, Northern Apennines (Italy)

The site of Loiano is in the Northern Apennines (Emilia-Romagna region, Italy), 20 kilometers to the south of the city of Bologna (Fig. 1a). The Northern Apennines are an orogenic wedge formed in response to the Upper Cretaceous-Eocene closure of the Ligurian-Piedmont ocean (Marroni et al., 2017) and the subsequent Oligocene-Miocene convergence and collision between the Adriatic Promontory and the Sardinia-Corsica Block, of African and European origin, respectively (Vai and Martini, 2001). Our work focused on the Loiano Sandstones of the Epiligurian Successions (Fig. 1a-c), the Middle Eocene to Middle Miocene siliciclastic infill of thrust-top, piggy-back basins discordant to the underlying Ligurian units, which migrated passively to the NE during the Apennines orogeny atop of the entre orogenic wedge. The 300-1000 m thick, Late Lutetian-Bartonian Loiano Sandstones are a fan-delta to proximal turbidite deposit (Papani, 1998). They are medium- to coarse-grained, poorly consolidated, immature arkosic sandstones and conglomerates deposited in a relatively small lenticular basin (a few tens of km in width and length; Fig. 1a, c). They are composed of 49 to 60% quartz and of 39–48% feldspar, the rest being rock fragments, detrital carbonate clasts, and minor accessories (Del Sole and Antonellini, 2019).

2.2 Bollène field site, Southeast Basin (Provence, France)

The site of Bollène is in the Southeast Basin of Provence (France), 15 kilometers to the north of the city of Orange (Fig. 2a). The Southeast Basin is a triangular region between the Massif Central to the north-west, the Alps to the east, and the Mediterranean Sea to the south. It is a Mesozoic cratonic basin on the edge of the Alpine orogen, approximately 200 km long and 100 to 150 km wide. Three main tectonic episodes affected the region (Arthaud and Séguret, 1981; Roure et al., 1992; Séranne et al., 1995; Champion et al., 2000): SSW-NNE Pyrenean contraction from Paleocene to Oligocene, NW-SE Gulf of Lion extension from the Oligocene to early Miocene (rifting), and, lastly, SW-NE Alpine contraction from Miocene to Quaternary (Fig. 2a). The site of Bollène is exposed in a quarry (Figs. 2c) located in Turonian sand (low cohesion sandstone), between 10 and 200 m thick in thickness and is situated north of the E-W Mondragon anticline (Fig. 2b, c). The Turonian sands at the Bollène quarry are laminated, fine to coarse grained with modal and bimodal grain size distributions; they formed in deltaic and aeolian environments. The host sands are not cemented. They are composed of 88 to 92% quartz, the rest being feldspar. The median grain diameter (D_{50}) is 0.31 mm, i.e. medium sand. Their porosities range from 20 to 43%, and the precise value at study site is 22.05% (Ballas et al., 2014).

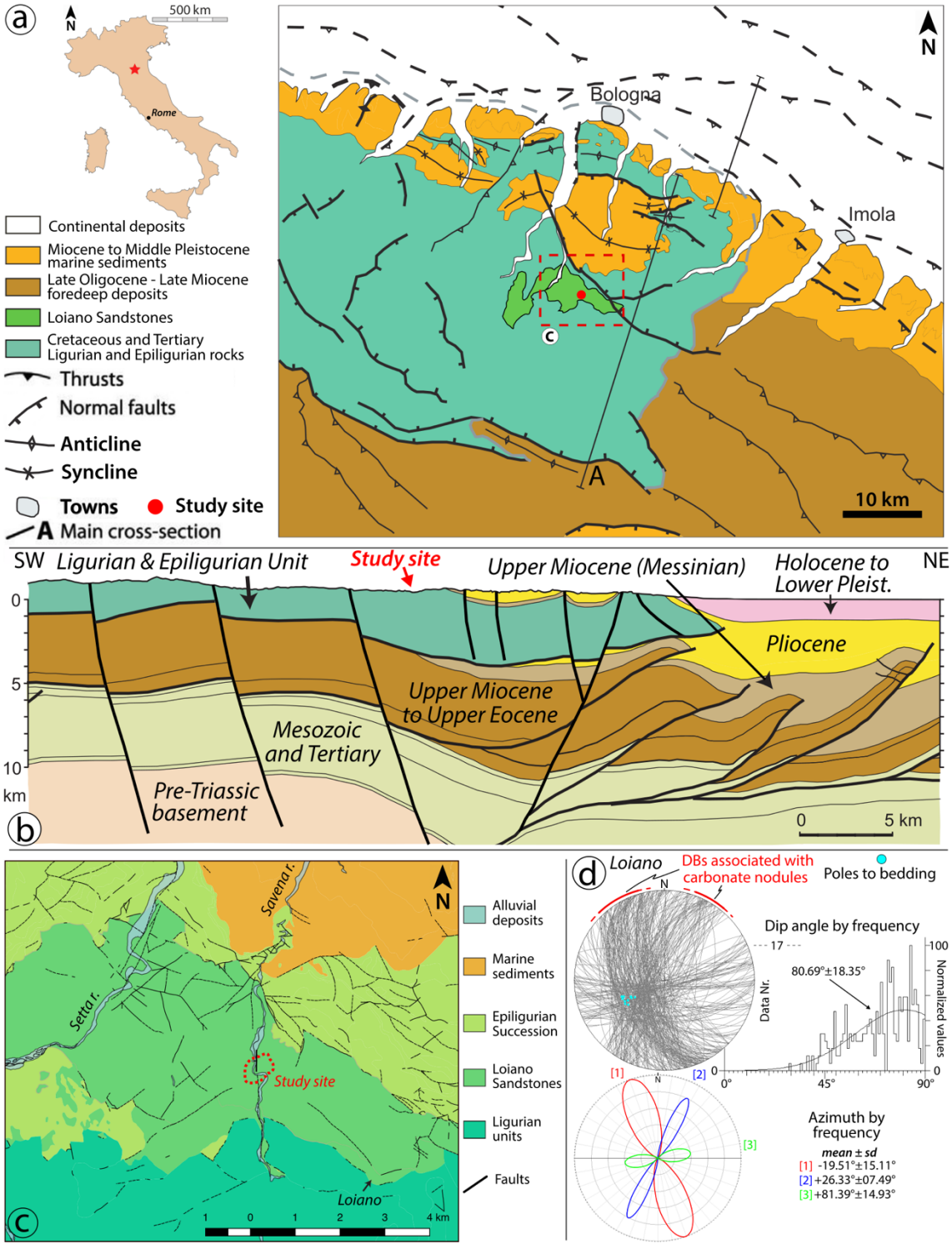
a
500 km
N
Rome
Continental deposits
Miocene to Middle Pleistocene marine sediments
Late Oligocene - Late Miocene foredeep deposits
Loiano Sandstones
Cretaceous and Tertiary Ligurian and Epiligurian rocks
Thrusts
Normal faults
Anticline
Syncline
Towns
Study site
A Main cross-section
Bologna
Imola
c
A
10 km
SW
Ligurian & Epiligurian Unit
Study site
Upper Miocene (Messinian)
Holocene to Lower Pleist.
NE
Pliocene
Upper Miocene to Upper Eocene
Mesozoic and Tertiary
Pre-Triassic basement
0
5
10
km
b
0
5 km
Savena r.
Setta r.
Study site
Loiano
c
1 0 1 2 3 4 km
Alluvial deposits
Marine sediments
Epiligurian Succession
Loiano Sandstones
Ligurian units
Faults
d
Loiano
DBs associated with carbonate nodules
Poles to bedding
Dip angle by frequency
17
100
80.69°±18.35°
Data Nr.
Normalized values
0
0°
45°
90°
[1]
[2]
[3]
Azimuth by frequency
mean ± sd
[1] -19.51°±15.11°
[2] +26.33°±07.49°
[3] +81.39°±14.93°

120

Figure 1. (a) Schematic geologic map and (b) cross-section of the Northern Apennines near Bologna (Italy), modified from Picotti and Pazzaglia, 2008. (c) Geologic map of the study area and location of the studied outcrops (red dotted line). This map is constructed from data of the *Regione Emilia-Romagna* (http://www.regione.emilia-romagna.it/). Location of (c) is indicated by a red square in (a). (d) Lower-hemisphere equal-area projection indicates the orientation of the different sets of DBs (298 data points) and poles to bedding at the study site. DBs associated with carbonate nodules are highlighted by a red line. DBs azimuth (strike; N ± 90°) frequency rose diagram and dip angle (°) plotted against frequency. Best-fit Gaussian curves superimposed on the corresponding data histograms (frequency distributions). Gaussian peaks and related standard deviations (± sd) are indicated for each population.

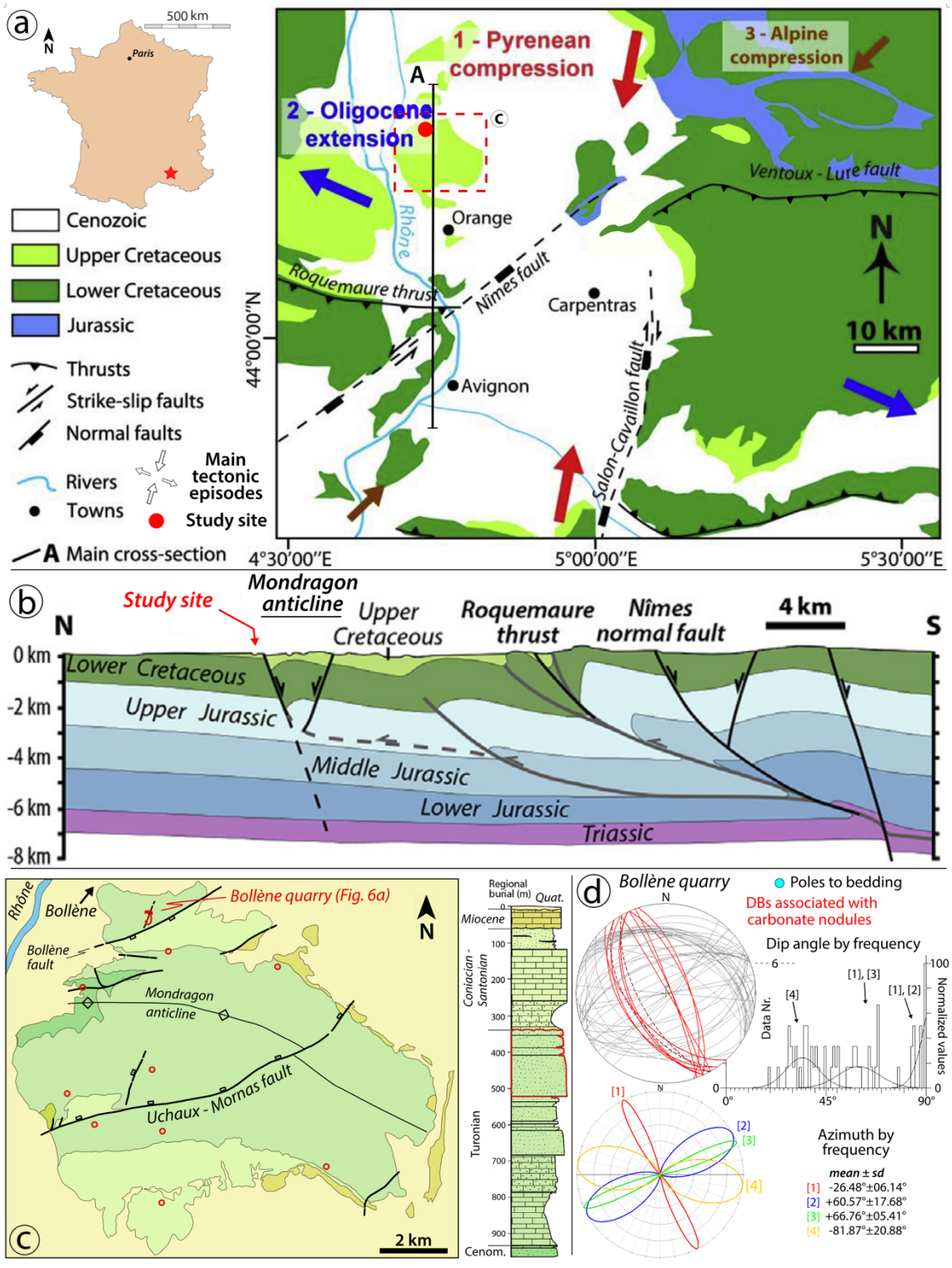
a
500 km
N
Paris
Cenozoic
Upper Cretaceous
Lower Cretaceous
Jurassic
Thrusts
Strike-slip faults
Normal faults
Rivers
Towns
Main tectonic episodes
Study site
A Main cross-section
1 - Pyrenean compression
2 - Oligocene extension
3 - Alpine compression
A
C
Rhône
Orange
Ventoux - Lure fault
Roquemaure thrust
Nîmes fault
Carpentras
Avignon
Salon-Cavaillon fault
N
10 km
44°00'00"N
4°30'00"E
5°00'00"E
5°30'00"E
b
Study site
Mondragon anticline
Upper Cretaceous
Roquemaure thrust
Nîmes normal fault
4 km
N
S
0 km
-2 km
-4 km
-6 km
-8 km
Lower Cretaceous
Upper Jurassic
Middle Jurassic
Lower Jurassic
Triassic
c
Rhône
Bollène
Bollène quarry (Fig. 6a)
Bollène fault
Mondragon anticline
Uchaux - Mornas fault
N
2 km
Regional burial (m)
Quat.
Miocene
Coniacian - Santonian
Turonian
Cenom.
d
Bollène quarry
Poles to bedding
DBs associated with carbonate nodules
Dip angle by frequency
Data Nr.
Normalized values
[1], [3]
[1], [2]
[4]
Azimuth by frequency
mean ± sd
[1] -26.48°±06.14°
[2] +60.57°±17.68°
[3] +66.76°±05.41°
[4] -81.87°±20.88°

Figure 2. (a) Schematic geologic map and (b) cross-section of the South East Basin, Provence, France. The main tectonic episodes affecting the region are reported in (a). (c) Geologic map and stratigraphic column of the Bollène quarry. Location of map in (c) is indicated by a red square in (a), and red open circles indicate some of past studies locations (see Wibberley et al., 2007; Saillet and Wibberley, 2010; Ballas et al., 2012, 2013, 2014; Soliva et al., 2013; Philit et al., 2018). (a), (b), and stratigraphic column in (c) are modified from Philit et al., (2015, 2018). Geological map in (c) is modified from Ballas et al. (2012). (d) Lower-hemisphere equal-area projection indicates the orientation of the different sets of DBs (64 data points) at the study site. DBs associated with carbonate nodules are highlighted in red. Dotted lines indicate the main attitude of tabular carbonate nodules. DBs azimuth (strike; N ± 90°) frequency rose diagram and dip angle (°) plotted against frequency. Best-fit Gaussian curves superimposed on the corresponding data histograms (frequency distributions). Gaussian peaks and related standard deviations (± sd) are indicated for each population. Number in square brackets [n] are the same as used in Fig. 6b to rank different sets of DBs.

3 Methods

3.1 Outcrops analysis

The geometry and distribution of DBs and nodules were documented by detailed field mapping at different scales for both sites. At the Loiano site, a map (370 m^2) at the 1:25 scale (1 cm ≃ 4 m) was made by standard topographic compass and tape mapping (Fig. 3). The Bollène quarry site pavement was mapped using a DJI PHANTOM™ drone. Photographs were taken at different altitude above the ground surface and were then used to build a 3D mesh and extract high-resolution orthophotos using *Agisoft PhotoScan Metashape* software (© Agisoft LLC). The high-resolution orthophoto mosaic (1 px ≃ 1-1.5 mm) was used for the detailed mapping of DBs and nodules. Furthermore, DBs and nodule patterns, as well as their characteristics and spatial relationships, were documented in the field on high-resolution photographs (15 megapixels), both in Loiano (Figs. 4 and 5) and Bollène (Figs. 7 and 8). Oriented samples were collected for thin section preparation, microstructural, and stable isotopes analysis. The orientation and dip of DBs were measured at each site and plotted in lower hemisphere equal area stereograms, rose diagrams, and frequency histograms (Figs. 1d and 2d) using the *Daisy3* software (Salvini, 2004).

3.2 Microstructural analysis

Polished thin sections of host sandstones, DBs, and nodule samples were analyzed by natural-light optical microscopy, cold cathodoluminescence, and backscattered electron imagery using a JEOL JSM-5400, and a FEI Quanta FEG 200 environmental scanning-electron microscope (SEM). These microscopy techniques were used to examine the texture and microstructures of host rock and DBs, as well as the cement distribution and texture (Figs. 9, 10, and 11). In particular, cold cathodoluminescence (CL) analysis of carbonate cement in nodules was conducted with a CITL Cold cathodoluminescence 8200 Mk5-1 system (operated at 14-15kV beam energy and 250µA beam current) equipped with a standard petrographic microscope (Olympus BH41). CL was used to describe the cement-crystals properties (texture, fabric,

luminescence) and the micron-scale spatial distribution and textural relationship among the cements, framework detrital grains, and the fractures (*sensu lato*). This information is used to (i) understand the interrelation between deformation, fluid flow, and diagenesis (e.g. cement precipitation); (ii) assess the relative timing of each process; (iii) describe porosity evolution with time; and (iv) understand the mechanisms and the geochemical environment of cement precipitation when coupled with other tools (e.g. stable isotopes analyses). The CL features (color, brightness) of the carbonate minerals are controlled primarily by the relative abundances of Mn^{2+}, REEs, and Fe^{2+}. These differences, in turn, reflect specific physio-chemical conditions of formation waters during mineral growth, including fluid chemistry (salinity), pH/Eh, temperature, pressure, ions activity, biological activity (e.g. Marshall, 1988; Barnaby and Rimstidt, 1989; Machel, 2000; Hiatt and Pufahl, 2014).

3.3 Stable isotope characterization

Stable carbon and oxygen isotope data from cements from within carbonate nodules were used to constrain the geochemical environment of precipitation and possible source of fluids. Powder samples for bulk rock carbon and oxygen stable isotopes analysis were ground with a dental drill from not weathered or altered sections of the nodules. A total of 46 sites were sampled from nodules in Loiano (n=30; Fig. 12a) and Bollène (n=16; Fig. 12b). Powders samples were analyzed with a Thermo Finnigan DELTA plus XP mass spectrometer coupled with a Thermo Finnigan Gas Bench II gas preparation and introduction system. $\delta^{13}C$ and $\delta^{18}O$ are referred to the international standard V-PDB (Vienna-Pee Dee Belemnite). Isotope determination analytical precision was 0.10‰ and 0.15‰ V-PDB for carbon and oxygen, respectively. The prediction uncertainty was c. 0.15‰ for carbon and c. 0.20‰ for the oxygen isotopes.

4 Deformation bands and cement: field observations

4.1 Loiano

At the study site, bedding strikes NW-SE and dips at an average of 38° to the NE (Fig. 1d). Deformation bands cluster into three different trends striking N20°W (NNW-SSE), N26°E (NNE-SSW to NE-SW), and N81E° (ENE-WSW) (Fig. 1d). All DBs dip moderately to steeply mostly in the west and south quadrants (Fig. 1d). Deformation bands commonly occur with a positive relief and appear as whitish linear traces with minor undulations forming eye and ramp structures, where they branch and merge (Figs. 3 and 4). Already at the outcrop they exhibit a significant reduction in grain size and porosity in comparison to the surrounding host rocks (Fig. 4f). Deformation bands occur both as single features and as clusters or zone of bands, i.e. in narrow zones with variable thickness (0.8-60 cm) with sub-parallel DBs (up to 40). Single DBs accommodate minor offsets from a few millimeters up to 40 mm, whereas clusters can accommodate offsets up to 0.5 m (Fig. 4b, d). Deformation bands display a variety of apparent normal and strike-slip offsets (Fig. 3). Different sets of DBs

show ambiguous and conflicting crosscutting relationships. Field observations indicate that the NNW-SSE and NNE-SSW sets have mutual crosscutting relationships typical of faults forming synchronously (Fig. 3).

The peculiar characteristic of the Loiano Sandstones is the occurrence of spatially heterogeneous carbonate cement in the form of isolated or multiple spheroids or irregular nodules and continuous tabular nodules (Figs. 4 and 5). The nodules weather out in positive relief, because they are more resistant to weathering than the weakly cemented host rock. Isolated nodules range in diameter (major horizontal axis) from 0.2 m to 3 m (Fig. 4c, d) whereas tabular concretions have a thickness ranging from 0.10 to 0.8 m and a long axis ranging from 3 up to 15 m in length (Fig. 5a). Generally, the nodule shape in Loiano is similar to that of an oblate spheroid. There is no evidence of spherical nodules or prolate spheroids. The volume of the carbonate nodules ranges from 0.001 m^3 to > 10 m^3. Nodules form about 20% of the exposed outcrop volume. Two types of nodules can be distinguished depending on whether they are associated with DBs or clusters (i.e. DBs-parallel nodules; Figs. 3, 4, and 5a-c) or with bedding planes (i.e. bedding-parallel nodules; Figs. 3 and 5d, e). The former represent roughly 75% of the total nodules in the study area and are the main target of this work. The association between DBs and nodules occurs in the form of (i) parallelism and spatial overlap between DBs and nodules and (ii) confinement of the nodules by the DBs. In all cases, nodules are oriented with the major axis (elongation direction) parallel to the DBs and the minor-axis (i.e. thickness) perpendicular to them. Deformation band-parallel nodules are isolated ellipsoids (Fig. 4b, d), or, alternatively, continuous tabular objects (Figs. 4a and 5a). Nodules may be located along the DB (or zone of bands) trace (Figs. 4a, d and 5a, b), placed in between and confined by DBs (Figs. 4b, e, and 5c), or they may be asymmetrically placed on one side of the DBs (Figs. 4c and 9e). In some cases, nodules lie at the intersection of different DBs planes (Fig. 3). Some DBs are not spatially associated with nodules (Figs. 3 and 4b). Among the multiple sets of DBs, those mostly associated with carbonate nodules are the NNW-SSE and the NNE-SSW one. As a result, most nodules are elongated along these two structural directions (Figs. 1d and 3; see also Fig. 1b in Del Sole and Antonellini, 2019). The other sets are rarely associated with carbonate nodules. Nodules are never cut across by the DBs.

Bedding-parallel nodules are either isolated (Fig. 3), multiple but laterally discontinuous (Figs. 3 and 5d, e), or laterally continuous layers with a tabular geometry (Fig. 3; e.g. “nodular beds” in Del Sole et al., 2020). Nodular beds are continuous pervasively-cemented layers that extend along the bedding plane for several meters (up to 15 m in length) and a nearly constant thickness of c. 35-50 cm. Nodules along bedding planes are more rounded and with gentle boundaries (Fig. 5d, e) than those associated with DBs, which are, instead, more tabular and exhibit angular and sharp boundaries (Figs. 4 and 5a-c). In some cases, nodule geometry and elongation direction follow both bedding surfaces and DBs (Fig. 3). Nodules, despite being ubiquitous in the sandstone, are mostly observed within coarse levels with grain size equal or larger than medium sands (0.25-0.5 mm). We did not observe any nodules in sedimentary rocks with grain size finer than sand (siltstone and clay). Bedding-parallel nodules are commonly located in sandstone levels confined between clay/silty levels or fine-grained-sand levels (Figs. 3 and 5d, e).

A set of joints and veins (Fig. 5a, b) were found exclusively within the carbonate nodules. They postdate DBs and nodules and do not propagate into the surrounding host sandstone.

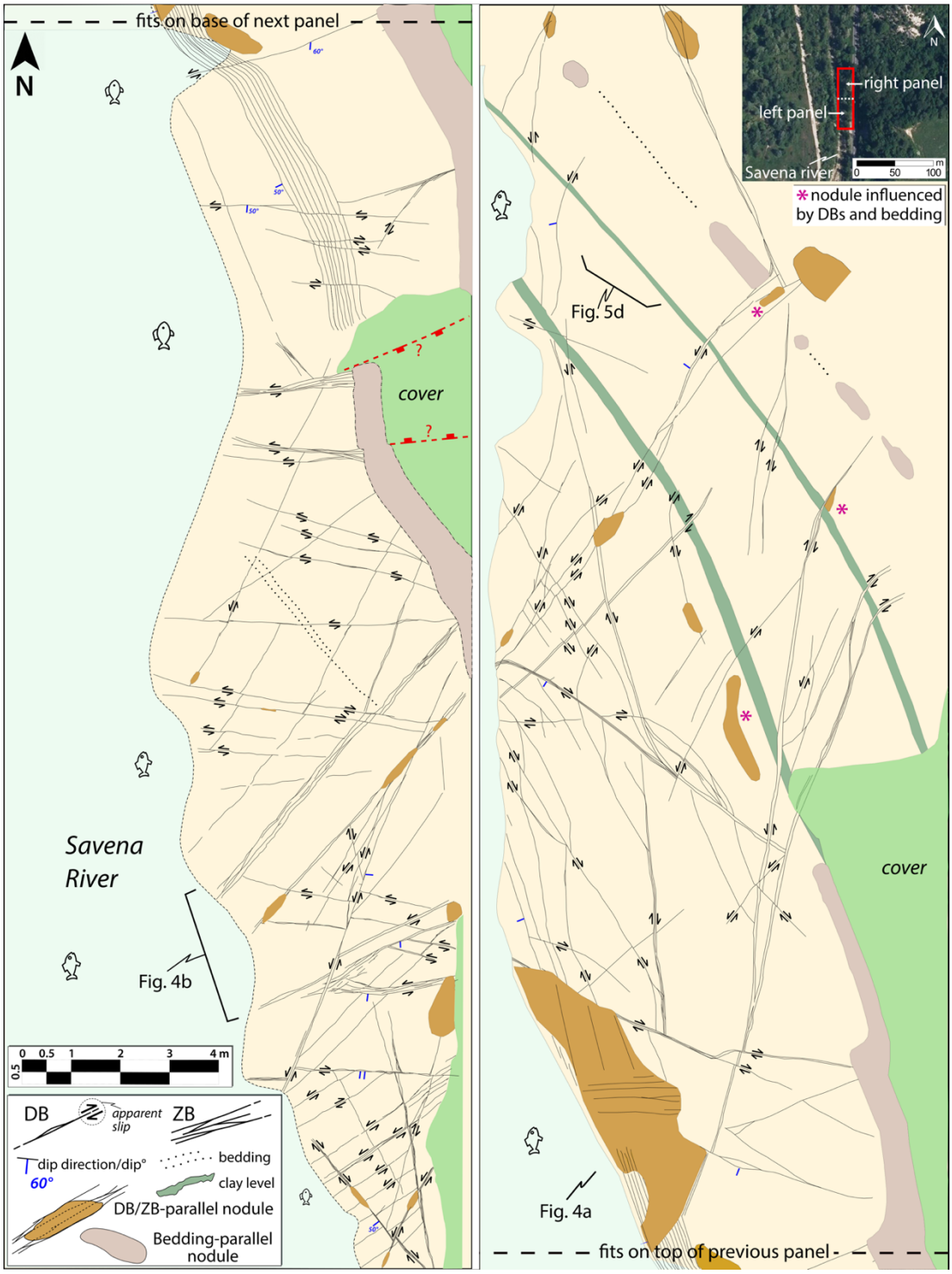
fits on base of next panel
N
cover
Savena River
Fig. 4b
0 0.5 1 2 3 4 m
0.5
DB
apparent slip
ZB
dip direction/dip°
60°
bedding
clay level
DB/ZB-parallel nodule
Bedding-parallel nodule
right panel
left panel
Savena river
0 50 100 m
*nodule influenced by DBs and bedding
Fig. 5d
cover
Fig. 4a
fits on top of previous panel

225

Figure 3. Outcrop map that documents geometry and distribution of DBs and nodules in a portion of the study area in Loiano. The right-hand panel fits on top of the left-hand panel. ZB – zone of bands. The inset (© Google Earth) shows the map location in the study area.

Figure 4. Relationships between nodules and DBs. Deformation bands occur either as single structures or organized in clusters (ZB). Nodules along DBs (or ZB) are isolated (b, d, e), or continuous with a tabular geometry (a). Nodules are located along the DB trace (a, b, d), or they are asymmetrically placed on a side of the DB (c). (e) Isolated nodule in between and confined by ZB. DBs are whiter than host rock, exhibit a positive relief, and a clear reduction in grain size and a lower porosity, both visible to the naked eye (f). The pen in (c, d) is 14 cm in length. The arrow-scale in (b, e) is 10 cm in length. The position of (a, b) is indicated in Fig. 3.

Figure 5. (a-c) DB-parallel- and (d-e) bedding-parallel nodules. (a) Decametric-scale continuous nodule with a tabular geometry located along a zone of bands (ZB). NE-dipping layering is shown with dotted lines. The photo is about 10 meters in depth. (b) Close-up on (a) from a map-view. The lens-cover is 5.5 cm in diameter. (a, b) Late opening-fractures cut through the assemblage "DBs – nodule" and they
240 do not propagate into the poorly consolidated host rock. (c) Isolated nodules placed in between and confined by ZB. (d, e) The bedding is

emphasized mostly by clay and silt horizons, sporadic well-defined thin levels of gravel, and the alignment of bedding-parallel nodules. (d) Black arrows point to multiple but laterally discontinuous bedding-parallel nodules. Here, a single DB (white line) crosses a bedding-parallel nodule without causing any offset. The position of (d) is indicated in Fig. 3. (e) Photomosaic showing a series of laterally-discontinuous nodules just below, above or in between several continuous impermeable clay-rich levels. The deformation pattern changes depending on the host rock properties (e.g. sorting degree, porosity ϕ, grain-size; see Supplement S1 for details). Cataclastic deformation is accompanied by clay smear (see inset) where DBs cut thin dark-colored clay levels.

4.2 Bollène

At Bollène, DBs occurs as belonging to three different trends oriented (i) NW-SE to NNW-SSE (set 1: N26°W; Figs. 2d and 6b), (ii) NE-SW to ENE-WSW (set 2: N61°E and set 3: N67°E; Figs. 2d and 6b), and (iii) ESE-WNW (set 4: N82°W; Figs. 2d and 6b). Trend (i) can be divided in two subsets; one is characterized by normal offsets NW-SE conjugate bands, moderate dip angles (50-60°) to SW (Figs.7a and 8a, c), and just a few to NE; a second one is characterized by dominant dextral strike-slip kinematic bands with higher dip angles (70-90°), and a NNW-SSE trend (Figs. 6b and 7f). Trend (ii) can be divided in two sets; one set is characterized by dominantly left-lateral and minor right-lateral subvertical strike-slip conjugate bands striking NE-SW to ENE-WSW (set 2 in Fig. 6b; Fig. 7a-c); a second set is instead characterized by a set of conjugate DBs with moderate dips (~60°), NE-SW orientation (set 3 in Fig. 6b), and undetermined kinematic (likely normal-sense). Trend (iii) is composed of ESE-WNW conjugate bands, with reverse kinematics and low dip angles (30-40°). In the field, DBs appear as whitish linear traces with minor undulations and characteristic eye structures where they branch and merge (Figs. 6b and 7). In most cases, DBs weather out in positive relief. Frequently DBs occur in narrow zones (a few millimeters up to 5-15 cm in thickness). Field observations indicate that ESE-WNW DBs are crosscut by NE-SW strike-slip DBs (Fig. 6b). The latter also crosscut also the NW-SE/NNW-SSE set (Fig. 7a-c, f). Bedding is oriented NW-SE and dips gently (<10°) to the S (Fig. 2b, d). Bedding is difficult to recognize on the floor of the quarry, because of its low dip and the massive texture of the rock (Fig. 6b). The Turonian sandstones outcrop on the quarry floor. There are two lithotypes. The first one is represented by massive porous sands with DBs and localized carbonate cementation (see description below). The second one is characterized by a massive calcrete level with tabular geometry (see Supplement S2 for details).

The Turonian Sandstones in the Bollène quarry are characterized by a spatially heterogeneous cementation (Fig. 6b). These diagenetic heterogeneities occur as spherical and tabular nodules (Figs. 7 and 8). Spherical nodules are arranged as isolated bodies within the surrounding host rock (Figs. 7c, g and 8a, d, e) or aggregated in tabular clusters (Fig. 7a, d). Nodules weather out in positive relief. Spherical nodules range in diameter from a few millimeters (0.004-0.005 m) to a few tens of cms (0.2 m), whereas tabular ones have a thickness ranging from a few cms to 0.1 m and a long axis up to 5 m in length (Figs. 6b and 7a-c). Assessment of nodules lateral extension is hampered by the presence of vegetation and debris cover whereas subsurface extension cannot be measured, because of the limited vertical exposures of the outcrops. Hence, the values reported here are minimum values. In general, the nodule shape may be approximated by a sphere where length, width, and thickness are “equal” and by an oblate spheroid where length and width are larger than the nodule thickness.

Carbonate nodule volume ranges from 10^{-7} (small spherical nodules) to > 2.5 m^3 (tabular nodules assuming length = width = 5m, and thickness = 0.1m). In Bollène, the nodules are all spatially and geometrically associated with DBs (i.e. DBs-parallel nodules; Figs. 6b and 7). This association occurs in the form of (1) parallelism between DBs and nodules, (2) geometric congruence between the DBs trend and the nodule (or nodules cluster) shape, and (3) confinement of nodules in parallel-to-bands compartments. In all these cases, tabular nodules and clusters of spherical nodules are oriented with the major axis (elongation direction) parallel to the DBs and the minor-axis (i.e. thickness) perpendicular to them (Figs. 7a and 8a). Unlike what we have seen in Loiano, in Bollène nodules are in compartments among DBs. Carbonate nodules are associated with the NW-SE/NNW-SSE DBs set (Figs. 6b and 7a, f). Although this set is conjugate with bands dipping to the SW and to the NE, the tabular cement bodies dip only to the SW (Figs. 2d and 8a-c). No nodules are cut by the NW-SE bands. The NE-SW/ENE-WSW strike-slip bands cut through the NW-SE/NNW-SSE bands and the associated NW-SE-trending carbonate nodules (Figs. 7a-c, f). There is clear evidence of these crosscutting relationships both at the outcrop and at the micro-scale (see Sect. 5.2). For this reason, we focus on the NW-SE DBs and nodules in the remaining part of this study.

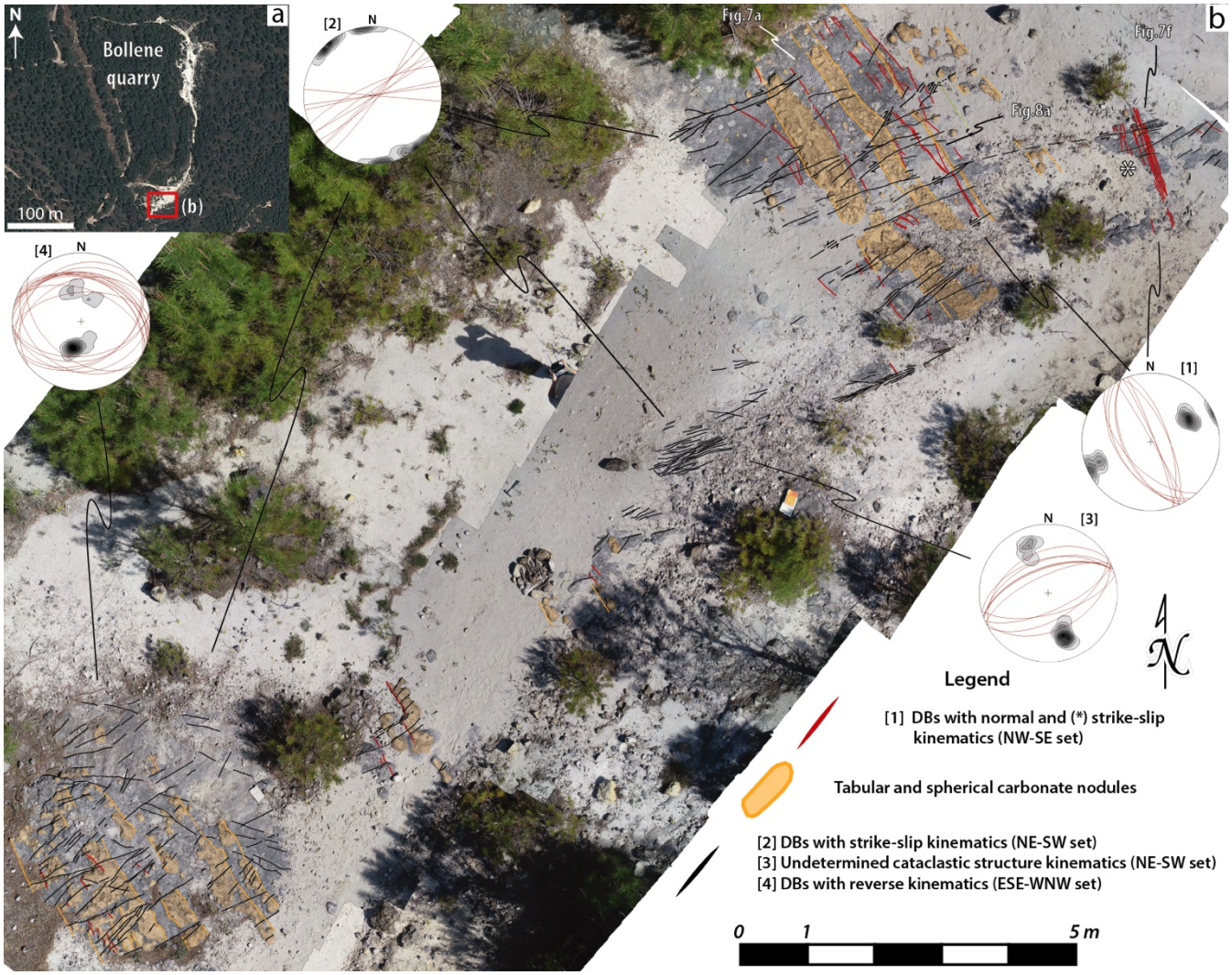

Figure 6. (a) Aerial photograph of the study site (© Google Earth). (b) Orthophoto that documents geometry and distribution of DBs and carbonate nodules in the Bollène quarry. Lower-hemisphere equal-area projection indicating the orientation of the cataclastic structures measured in (1) NW-SE/NNW-SSE normal and (dextral) strike-slip bands associated with tabular and spherical nodules; (2) NE-SW/ENE-WSW strike-slip bands; (3) NE-SW bands with undetermined kinematics; (4) ESE-WNW reverse-sense bands.

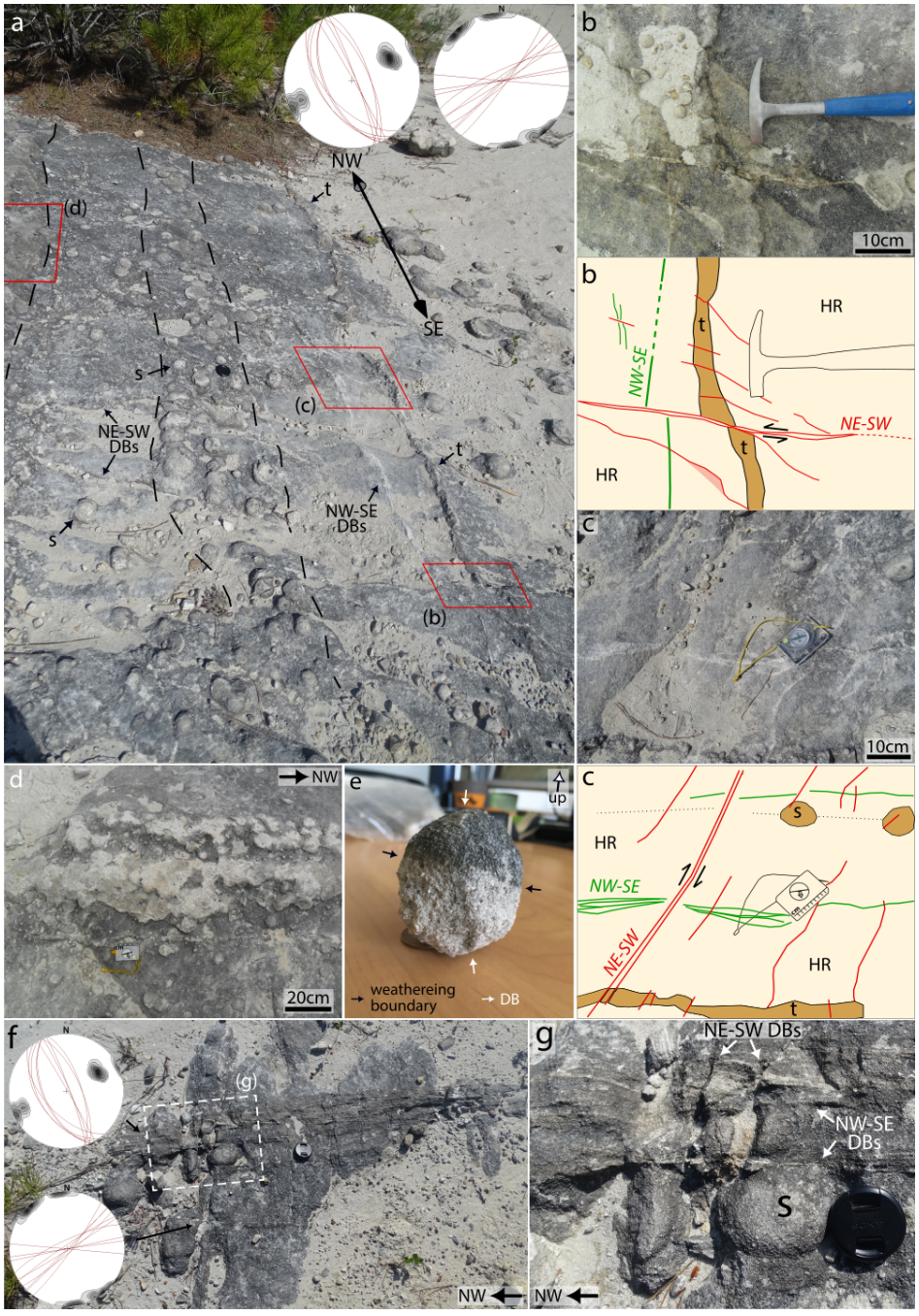

Figure 7. Calcite cement occurs in the form of isolated (a, c, g) or clusters (a, d) of (S) spherical nodules and continuous (t) tabular nodules (a-c). Nodules are arranged in compartments parallel to clusters of NW-SE normal bands (a-c) and to NNW-SSE dextral strike-slip bands (f, g). NE-SW/ENE-WSW strike-slip bands displace both the NW-SE bands and their associated nodules (a-c, f). (e) Spherical nodule (about 5 cm in diameter) in spatial superposition with a NW-SE DB that does not displace the cement. Lens-cover in (a, f) has a 5.5 cm diameter. The figures (a-d, f, g) are in map-view. The position of (a, f) is indicated in Fig. 6b. Hammer length in (b) is 30.5 cm.

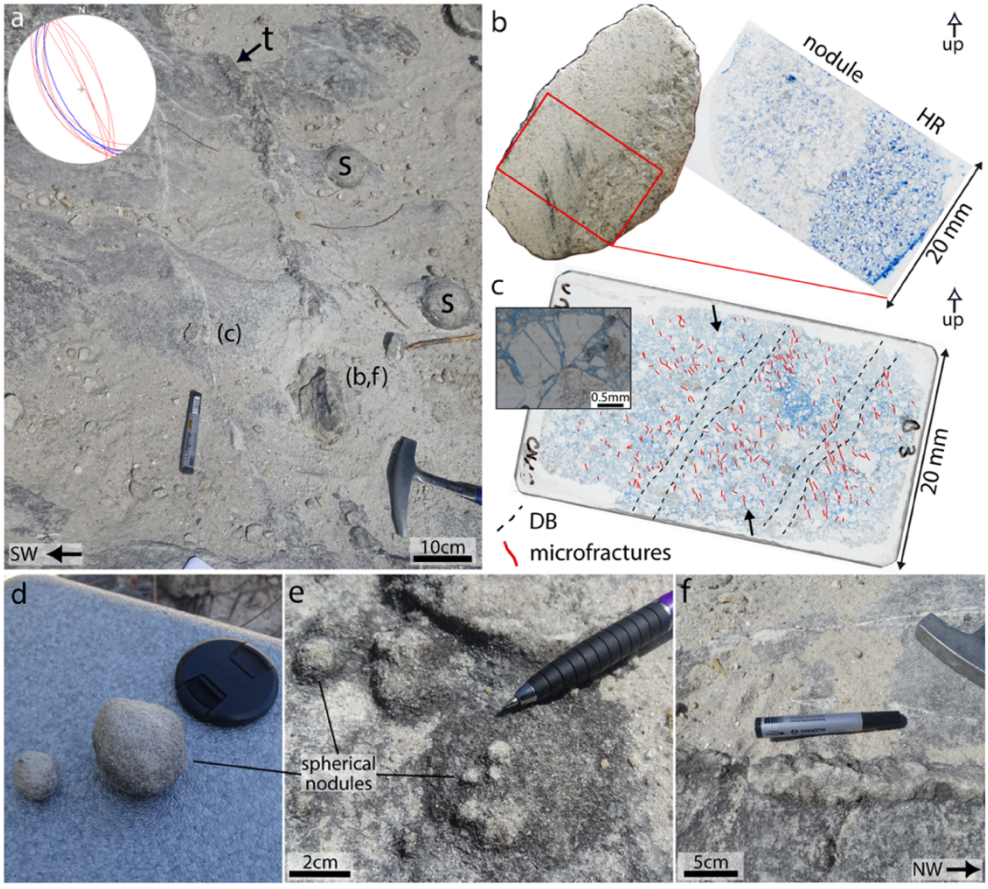

Figure 8. Typical relationships between nodules and DBs. (a) Continuous tabular nodule (t) and isolated spherical nodules (S) aligned parallel to the NW-SE normal-sense bands dipping SW (~55°; red lines in the inset stereoplot). The tabular bodies dip to the SW parallel to the bands (blue lines in the stereoplot in the inset). The position of (a) is indicated in Fig. 6b. (b) Hand specimen and polished thin sections impregnated with blue-dyed resin of a tabular nodule in (a). (c) Polished thin sections impregnated with blue-dyed showing two sub-parallel NW-SE normal-sense bands dipping SW. Mapping of microfractures developed at grain contacts consistent with Hertzian contacts (e.g. Eichhubl et al., 2010; Soliva et al., 2013) endorses the normal kinematic of these bands (see Supplement S1 for details). "Up" refers to the topography. Close-up on spherical (d-e) and tabular (f) nodules from the field. Pen-marker length in (a, f) is about 13.5 cm. Lens-cover in (d) has a 5.5 cm diameter.

5 Deformation bands and cement: textural and microstructural characteristics

5.1 Loiano

Host rock total porosity (minus-cement ϕ) is between 20-26% (Fig. 9; Del Sole and Antonellini, 2019). Porosity is predominantly intergranular, whereas intragranular (e.g. pores within bioclasts) and "oversize" pores are due to dissolution

of detrital grains (Figs. 9 and 10). Deformation band total porosity (minus-cement ϕ) is lower by an order of magnitude (below 5%) than the host rock porosity (Fig. 9d). In the nodules, the host rock porosity is almost completely filled by cement (Fig. 10), so that the remnant porosity (voids) is low (down to 1.3%) (Fig. 9a, c). The presence of cement within the DBs enhances the porosity reduction caused by grain crushing and compaction (Fig. 9d). The microstructure of the DBs is characterized by reduced of grain size, porosity and pore size than in the host rock (Fig. 10i-l). Within the DBs a few coarse grains are surrounded by a fine-grained matrix.

Despite the different effects of mechanical and chemical compaction and minor authigenic alterations (refer to Supplement S1 for details), the major diagenetic components of the Loiano Sandstone are calcite cements. These cements fill mainly intergranular, and at lesser extent intragranular (intraskeletal) pore spaces, intragranular fractures, and they encase the framework grains and all other diagenetic features. Bedding-parallel nodules (Fig. 10a-h) are characterized by a mosaic texture of blocky sparite to poikilotopic bright-orange to orange-CL calcite cement. Crystal-size is typically 40-100 μm and up to 300 μm (Fig. 10g, h). This cement phase is the most widespread one and it is almost everywhere uniform in terms of texture and CL-pattern, if not for some minor dark-CL sub-zones (Fig. 10g, h). A minor calcite cement phase is associated with detrital carbonates (bioclasts) and it shows a bright-orange CL (Fig. 10c-d). It occurs as pore-lining formed by elongate and sharp rhombohedral shape calcite (dogtooth) that outlines the outer rim of the bioclasts (Fig. 10c) and drusy mosaic calcite that fills intraskeletal pores, outline bioclasts, and fills intragranular fractures in bioclasts (Fig. 10d). This subordinate phase was observed only in bedding-parallel nodules. Pore-lining cement around bioclasts is present only where there was pore-space (now filled), whereas it is absent where other grains are in contact with the bioclast. All cement phases described above (intergranular, intraskeletal, and pore-lining) encase compacted grains, and cements are undeformed still preserving the original shape. Pore-filling cement in DBs-parallel nodules (Fig. 10i-n) show a similar texture and CL-pattern to that described for the main intragranular cement phase in the bedding-parallel nodules (Fig. 10a-h). The main features that differentiate DB-parallel nodules from bedding-parallel ones are the finer crystal size of calcite within DBs, (Fig. 10i-l) and the absence of a bright-orange CL cement phase described in association to bioclasts in bedding-parallel nodules (Fig. 10c, d). Some bright-orange CL cement was observed only in detrital form (crushed) within the DB (Fig. 10k). The pore filling in DBs is fine-grained sparite; no evidence was found of crushed calcite crystals belonging to the dominant calcite phase. The finer fraction within the DBs is a matrix made up of comminuted angular and fine-grained clasts (flakes) of feldspar and in a smaller degree quartz, encased by the cement (Fig. 10j-l). Similarly, the cement fills the microfractures that cut through coarser grains and it encase the fine-grained clasts that are present within these fractures. Although, these microfractures are frequent in the host rock sectors in proximity to the DB (Fig. 10i), they were observed also in bedding-parallel nodules (Fig. 10a, b). Host rock volumes within DBs-parallel nodules are still characterized by blocky sparite cement with some minor dark-CL growth sub zones (Fig. 10i, m, n), similarly to what was observed in bedding-parallel nodules.

To evaluate any sign of dissolution in nodules, we carefully checked cement crystals morphologies adjacent to poorly- or non-cemented host rock sectors at the edges of nodules. Here, cement crystals boundaries are regular and sharp (Fig. 10m, n).

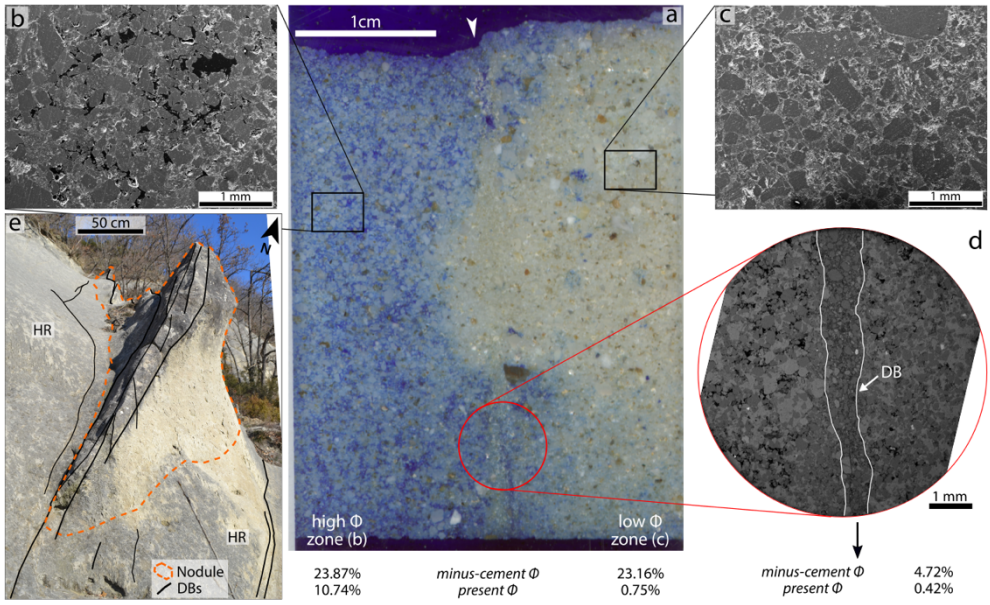

Figure 9. Host rock (HR) and DBs porosity and relationships between cement and DBs in Loiano Sandstones. (a) Polished thin sections impregnated with blue-dyed resin. The section shows a DB (arrow) separating two host rock sectors: in the right-hand side there is extensive calcite cementation whereas on the left-hand side cementation is poor. (b, c) Secondary electrons and (d) backscattered electrons SEM images from different sectors of the section (a). Porosity (ϕ) estimations data in (a-d) from Del Sole and Antonellini (2019). (e) Field example where a nodule is asymmetrically placed on a side of the DBs, similarly to what is observed in (a). See text for further details.

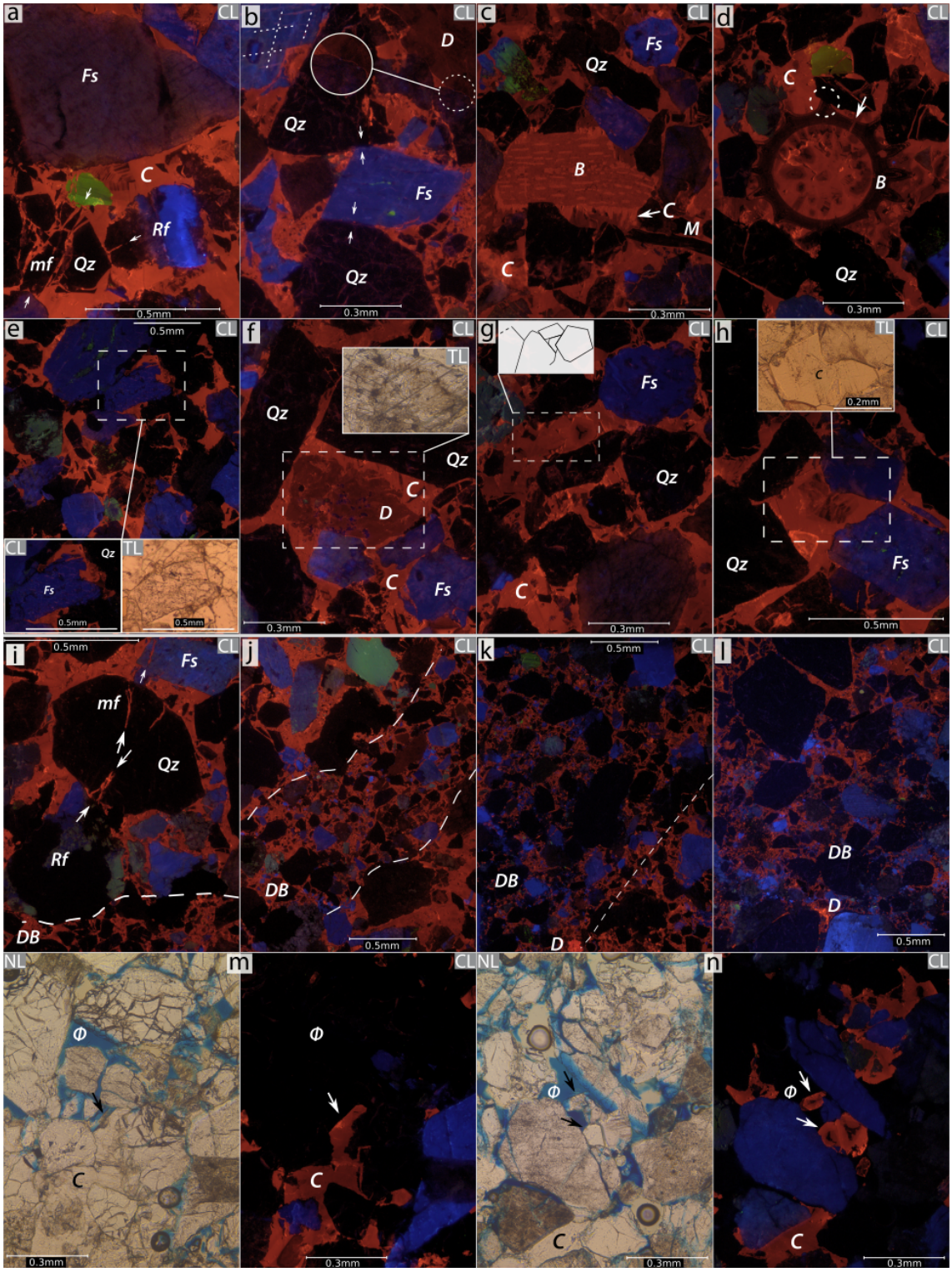
a
CL
Fs
C
Rf
mf
Qz
0.5mm
b
CL
D
Qz
Fs
Qz
0.3mm
c
CL
Fs
Qz
B
C
M
C
0.3mm
d
CL
C
B
Qz
0.3mm
e
0.5mm
CL
CL
Qz
Fs
0.5mm
TL
0.5mm
f
CL
TL
Qz
Qz
C
D
C
Fs
0.3mm
g
CL
Fs
Qz
C
0.3mm
h
TL
CL
C
0.2mm
Qz
Fs
0.5mm
i
0.5mm
CL
Fs
mf
Qz
Rf
DB
j
CL
DB
0.5mm
k
0.5mm
CL
DB
D
l
CL
DB
D
0.5mm
NL
m
CL
Φ
C
0.3mm
Φ
C
0.3mm
NL
Φ
C
0.3mm
n
CL
Φ
C
0.3mm

355

Figure 10. Natural- and CL-light photomicrographs showing the microstructure, and cement textures in (a-h) bedding-parallel and (i-n) DBs-parallel nodules. (a-b, d) Microfractures forms at grain contacts due to stress concentration at contact points. (i) Microfractures are common in the host rock areas close to the DB. (b) Feldspars break mainly by cleavage-controlled intragranular fractures (white dotted line). Some framework grains show planar to slightly undulated framework grain-to-grain contacts. Detrital carbonate clasts and (c-d) bioclasts are partially dissolved at grain contacts. (e) Some detrital grains are corroded and coated or partially replaced by cement. (f) Syntaxial overgrowth cement on a detrital carbonate clast (D). Bright-CL (c) circumgranular pore-lining (dogtooth texture) and (d) intraskeletal (drusy mosaic) calcite cement was observed only in bedding-parallel nodules. The main cement phase is characterized by bright-orange to orange-CL calcite cement that fills intergranular porosity and intragranular fractures both in (a, b, e-h) bedding-parallel nodules and (i-n) DB-parallel ones. (g-h, m-n) Host rock volumes in nodules are characterized by blocky sparite to poikilotopic calcite cement with minor dark-CL sub-zones, whereas (j-l) the cement in DBs is fine-grained sparite. (m-n) At nodules edges, cement crystal rims are regular and sharp suggesting absent or negligible dissolution. Bright grains in (k, l) are detrital calcite (D). Qz - quartz; Fs - feldspar; M - mica; Rf - rock fragment; B - bioclast; ϕ - pore space; C - calcite cement; TL - transmitted light. See text and Supplementary Material (S1) for further details.

5.2 Bollène

The host sands at Bollène are weakly cemented, with the exception of localized carbonate cementation described above. Host rock grains are mostly rounded and lack a fabric (Fig. 11a, f). Here, we describe the microstructure of NW-SE/NNW-SSE normal-sense and strike-slip bands, and NE-SW/ENE-WSE strike-slip bands sets. The most recognizable features that characterize both DBs sets are the reduction of grain size, porosity, and a tighter packing relative to the host rock (Fig. 11). NE-SW strike-slip bands (Fig. 11i-l) have a higher degree of grain comminution, porosity reduction, and tighter packing when compared to NW-SE bands (Figs. 8c and 11g-h). Most grains within the bands are fractured and angular. Despite the strong comminution, a few rounded large survivor quartz grains are preserved in the DBs matrix (Fig. 11g, h, k). Fine angular grains that are mostly comminuted feldspars fragments and secondarily quartz and minor oxides make up the matrix. We observed also fine particles of crushed calcite cement among the matrix grains within NE-SW bands (Fig. 11k, l). In some cases, the grains in the host rock areas in proximity to the DB are encased by relatively undeformed carbonate cement (Fig. 11i, j). Some grains in the host rock are corroded and partially replaced or coated by calcite cement (Fig. 11c).

The main cement in spherical and tabular nodules is a poikilotopic calcite that infills intergranular pores (Fig. 11a-e). Most of the cement is non-luminescent (dark luminescence) under CL (Fig. 11c, d) but a few crystals show partial overgrowths with bright-orange CL color (Fig. 11e). When the crystal has a heterogeneous CL-pattern, the non-luminescing zones are mainly in the crystal core whereas the luminescing sub-zones are mostly at the crystal edges (Fig. 11e). A very thin film (up to c. 10μ thick or less) of bright-orange CL calcite cement commonly coats the detrital grains (Fig. 11c), and it is visible also under natural-light (Fig. 11b). In the nodules, some of the intragranular microfractures at contact points are filled by cement (Fig. 11a); a few are not (Figs. 11b). The cements described above (pore-filling and grain-coating) are relatively

undeformed (i.e. no microfractures, no twin-lamellae) and still preserving the original shape, except where the NE-SE/ENE-WSW strike-slip bands crosscut the cement nodules. At the crosscutting site, indeed, and more specifically in the host rock sectors in proximity to the NE-SW/ENE-WSW bands, we observe intragranular fractures at contact points and the onset of cement comminution between quartz clasts (Fig. 11i, j). Fine particles of crushed detrital calcite cement are found among the cataclastic matrix grains within NE-SW/ENE-WSW strike-slip bands where they interact with nodules (Fig. 11k, l). At the microscale, no preferential or significant calcite cementation was observed in association with the NW-SE bands. The association between cements and these latter bands was observed only at the mesoscale (see Sect. 4.2).

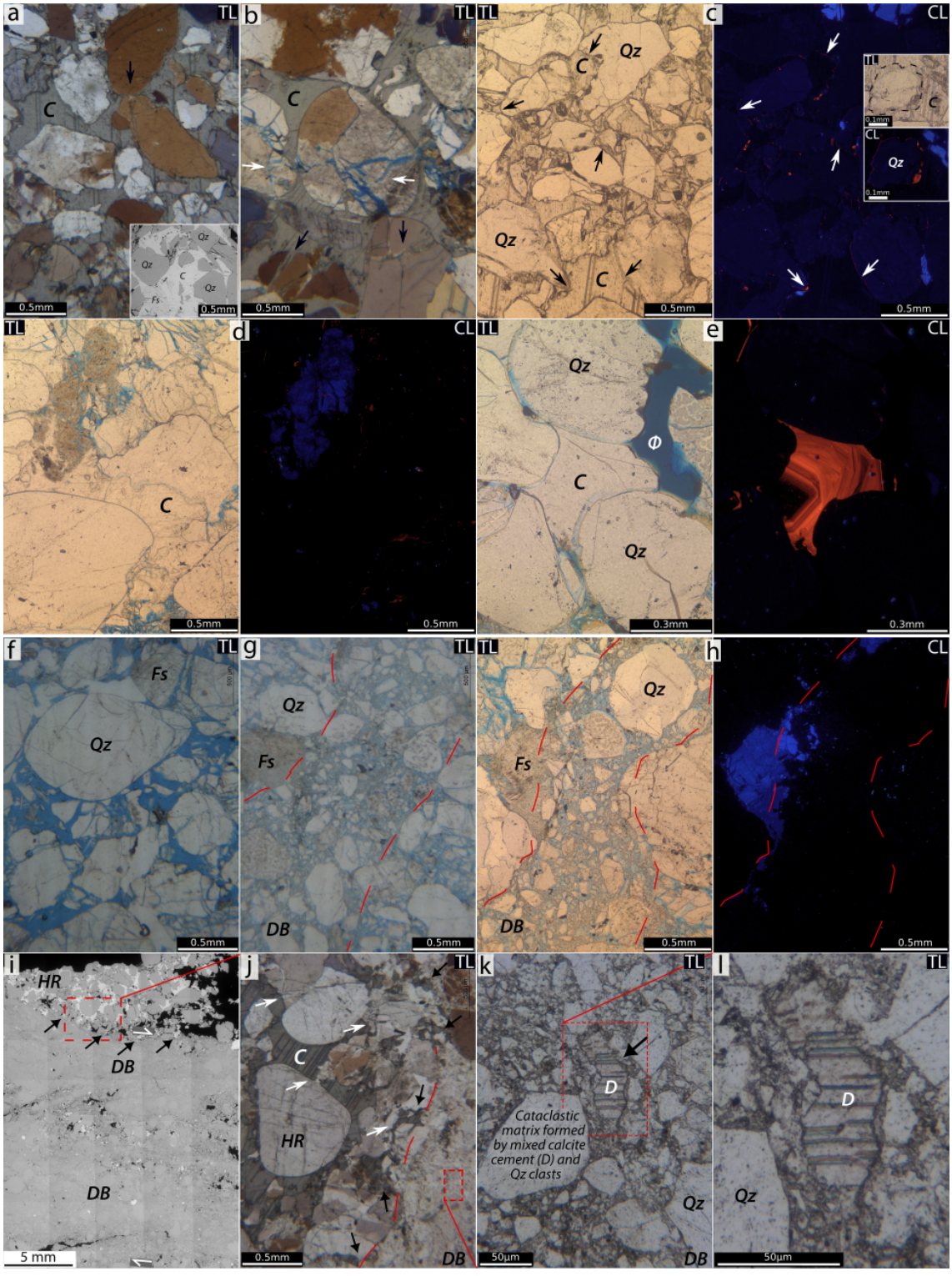
a
TL
C
Qz
Fs
0.5mm
b
TL
C
0.5mm
TL
C
Qz
Qz
C
0.5mm
c
CL
TL
C
0.1mm
CL
Qz
0.1mm
0.5mm
TL
C
d
CL
0.5mm
TL
Qz
Φ
C
Qz
0.3mm
e
CL
0.3mm
f
TL
Fs
Qz
0.5mm
g
TL
Qz
Fs
DB
0.5mm
TL
Qz
Fs
DB
0.5mm
h
CL
0.5mm
i
HR
DB
DB
5 mm
j
TL
C
HR
0.5mm
DB
k
TL
D
Cataclastic matrix formed by mixed calcite cement (D) and Qz clasts
Qz
50µm
DB
l
TL
D
Qz
50µm

Figure 11. Natural- and CL-light photomicrographs showing the internal texture and microstructure of (a-e) spherical and tabular nodules and (f-l) DBs. (a, b, f) Host rock grains are mostly rounded and nearly undisturbed. Some microfractures break framework grains at contact points. In nodules, (a) some of the microfractures are filled; (b) a few are not. (g, h) Microfractures are more frequent approaching the DB and (j) they are preferentially oriented with respect to the band (white arrows). Cement fills intergranular pore-space and intragranular fractures. (c-e) The major diagenetic component is poikilotopic spar cement with dominant dark-luminescence and (e) minor bright-orange CL growth sub-zones. (c) A very thin film of bright-orange CL calcite cement often coats detrital grains. Minor diagenetic alterations are corroded detrital grains that are partially replaced by calcite cement; see inset in (c). (g, h) NW-SE bands and (i, l) NE-SW strike-slip bands show a similar pattern, but NE-SW bands feature a high degree of grain comminution and porosity reduction. (i, j) NE-SW strike-slip bands crosscut cement nodules; intragranular fractures (white arrows) and incipient stage of cement comminution (black arrows) between quartz clasts in the host rock sectors in proximity these bands. (k, l) Fine particles of crushed detrital calcite cement (D) are found among the matrix grains at the crosscutting site. The inset in (a) is a backscattered electrons SEM image. Qz - quartz; Fs - feldspar; ϕ - pore space; C - calcite cement; TL - transmitted light. See Supplementary Material (S1) for details.

6 Cement stable isotopes geochemistry

6.1 Loiano

Cement from the nodules of the Loiano samples has $\delta^{13}C$ values between -7.68 and -1.47 ‰ (V-PDB) and $\delta^{18}O$ values between -4.42 and -1.35 ‰ (V-PDB) (Fig. 12a). The cement from DBs-related nodules is characterized by isotope compositions between -5.41 and -1.47 ‰ (V-PDB) for $\delta^{13}C$, and between -4.42 and -1.40 ‰ for $\delta^{18}O$ (V-PDB). The cement from bedding-parallel nodules has isotope compositions between -7.68 and -5.94 ‰ (V-PDB) for $\delta^{13}C$, and between -2.09 and -1.35 ‰ (V-PDB) for $\delta^{18}O$. Both cement groups (DBs-parallel and bedding-parallel nodules) have a relatively narrow range of oxygen isotopic composition featuring a near-vertical alignment in the $\delta^{18}O$–$\delta^{13}C$ cross-plot. DBs-parallel nodules show a slightly wider span of $\delta^{18}O$ composition when compared to bedding-parallel nodules. However, carbon isotopic composition shows a wide range of variability, both when considering the total isotopic composition data and when considering the cement groups data.

6.2 Bollène

Stable isotope analysis of the Bollène samples also defines two groups of data in the $\delta^{18}O$–$\delta^{13}C$ space (Fig. 12b). The cement group referring to the DBs-related nodules has $\delta^{13}C$ values between -7.73 m and -4.68 ‰ (V-PDB) and $\delta^{18}O$ values between -7.70 and -5.88 ‰ (V-PDB). The other group is from cement sampled in a calcrete level observed within the same Turonian sandstone few meters above the studied outcrop (see Sect. 4.2 and the Supplement S2 for details), and it is characterized by isotope compositions between -2.54 and -2.39 ‰ (V-PDB) for $\delta^{13}C$, and between -6.58 and -6.32 ‰ (V-PDB) for $\delta^{18}O$. Both cement groups have a relatively similar $\delta^{18}O$ signature and a relatively narrow range of $\delta^{18}O$ composition varying only between -7.70 and -5.88 ‰ (V-PDB). In a similar way, cement sampled from the calcrete has a

narrow range of $\delta^{13}C$ composition and show the heavier $\delta^{13}C$ values in the data set. However, $\delta^{13}C$ composition of DBs-related nodules has a wider variability range and is the most depleted in the data set.

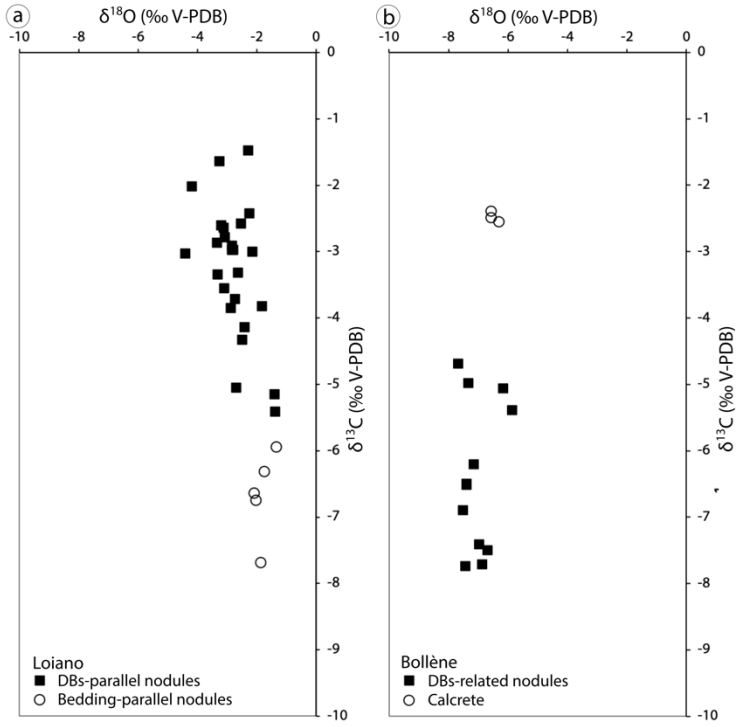

Figure 12. Stable isotopes analysis results. (a) Cumulative isotopic data characterizing the DBs-parallel nodules (black full-dots) and bedding-parallel ones (empty-dots) inside the Loiano Sandstones. (b) Isotopic data from the DBs-related nodules (black full-dots) and cement sampled in the calcrete (empty-dots) in Bollène quarry (see the Supplement S2 for details).

7 Discussion

In the following, we compare the two field sites highlighting their similarities and differences concerning the interaction between deformation, fluid flow, and diagenesis. We discuss the influence of DBs on fluid flow, their role in enhancing diagenesis and localizing diagenetic products (nodules). Finally, we propose an explanation for the geochemical environment within which fluids were sourced and precipitated the nodule cement. We then explore the implications of structural diagenetic heterogeneities (SHD) upon subsurface fluid flow and reservoir characterization.

7.1 Cement distribution and its relationship with deformation bands

The distinctive feature of the *Loiano Sandstones* is a spatially heterogeneous cementation in the form of nodules. Field evidence indicates that DB formation predates calcite cementation. All nodules are spatially related to DBs (Figs. 3 and 5a-c) except for those that are situated along bedding planes (~25% of the total nodules; Figs. 3 and 5d, e). In contrast, not all

DBs are associated with nodules. A clear correspondence always exists between shape and elongation direction of the nodules and the DBs direction. This pattern is observed also from aerial photographs (Del Sole and Antonellini, 2019). Localized cement along these structural features itself is an indication that deformation preceded cement precipitation (e.g. Eichhubl et al., 2004). If the sandstones were completely cemented at first, and then completely removed except from the DBs, the cement in the DB's matrix would most likely have been preserved in orange-reddish hues (oxidation residues); but nothing like that was observed. Moreover, cement morphologies adjacent to the porosity at nodules edges imply that cement dissolution has not occurred (Fig. 10m, n), thus excluding that nodules, both those parallel to bedding and those parallel to DBs, are relicts from an overall dissolution process. No DBs crosscut the cement, at least for those sets that are spatially related to nodules (NNW-SSE to NE-SW) indicating that cementation postdate DBs development. The precipitation of cement and (the consequent) lower porosity would favor the formation of joints over DBs in the sandstone (Flodin et al., 2003; Aydin et al., 2006; Fig. 5a, b). The presence of pore-filling cement would increase the strength of the sandstone (Del Sole et al., 2020), preventing rotation and sliding of particles, increase rock cohesion (Bernabé et al., 1992) and grain contact area, thus yielding a uniform contact stress distribution and higher stiffness (Dvorkin et al., 1991). Extensive cement, then, would inhibit DBs development. We can affirm, hence, that cement overprints the deformation bands.

Results from microstructural observations show that intergranular cement in the nodules encloses the grains both within host rock and DBs, and it overprints burial-related mechanical and chemical compaction features (Fig. 10a-h). These evidence point out that the formation of authigenic cements occurred after significant compaction (Cibin et al., 1993; Milliken et al., 1998). Estimated burial depths referred to the top of the Loiano Sandstones are 800-1000 m (Cibin et al., 1993) and 700-1200 m (McBride et al., 1995). Transgranular microfractures at grain contacts are due to stress concentration at contact points and they are interpreted as load-bearing structures within the granular framework (e.g. Antonellini et al., 1994; Eichhubl et al., 2010; Soliva et al., 2013). In DBs-parallel nodules samples the cement that fills the transgranular fractures is in continuity (i.e. same textural and CL characteristics) with the pore-filling cement outside the fractures. The presence of undeformed cement within structural-related features such as microfractures and crushed grains (Fig. 10i-l), both within and outside the DBs, proves that cement precipitation occurred after (at least after the early stages of) deformation.

The bands are the main controlling factor on the location, geometry, and elongation direction of DBs-parallel nodules. The occurrence and location of bedding-parallel nodules is controlled by grain-size and contrast in grain-size within the host rock. Although bedding-parallel nodules are found in all sands, they are more common within coarse-grained levels (≥ medium sands; i.e. size range: 0.25-0.5 mm). There are no nodules in sediments below the sand range or in layers with permeability below 100 mD (Del Sole et al., 2020). Moreover, bedding-parallel nodules are often restricted to sand level in contact above and/or below with clay/silty levels (Fig. 5d, e). Hence, grain size, and permeability variations are the most important factors controlling diagenetic and nodules formation in Loiano. The grain size and permeability variations as dominant control on nodules development in porous media is also reported by other authors (Mozley and Davis, 1996; Davis et al., 2006; Cavazza et al., 2009; Balsamo et al., 2012). In general, bedding-parallel nodules show a more rounded morphology when compared to DBs-related nodules. The former nodule type owns its smooth morphology to a

480 homogeneous and isotropic weathering; the sharp and squared shapes of DB-s parallel nodules is probably due to the anisotropy introduced by the DBs in the host rock that influences the cementation. The interplay between band strength and erosion may also be influent on nodule shape.

In the *Bollène quarry*, all calcite nodules occur in association with the DBs, and in particular with the NW-SE/NNW-SSE set (Fig. 6b). At this site, we observe complex relationships among multiple deformational and diagenetic
485 events. Timing of bands and nodules is inferred from crosscutting relationships. There is no evidence of low-angle ESE-WNW reverse-sense DBs crosscutting the cement nodules, whereas NE-SW to ENE-WSW trending strike-slip DBs offset the reverse-sense bands, the NW-SE bands, and the NW-SE-trending cement nodules (Figs. 6b and 7). The localization and parallelism between DBs and cement is similar in the two field sites, with the exception that NW-SE-trending nodules and DBs in *Bollène* are not superposed. Here, DBs are always overprinted by cement but the spatial overlap between DBs and
490 nodules (Fig. 7e) is unusual. Nodules occur in compartments that are spatially confined by DBs zones. Tabular nodules and clusters of spherical nodules are oriented with the major axis parallel to the NW-SE DBs (Figs. 6b and 7a). The NW-SE bands do not crosscut the cement, therefore, calcite cementation occurred between the NW-SE bands formation (Pyrenean contraction or Oligocene-Miocene extension?) and the NE-SW strike-slip bands (Miocene-Quaternary age Alpine shortening?). Please refer to Supplementary Material (S1) for details on how DBs relate to the tectonics of the area.
495 Microstructural observations show that the dominant phase of intergranular calcite cement encloses the grains within the nodules and it overprints only a proportion of the transgranular microfractures at grains contact points. All microfractures in the nodules are filled by a cement that is in continuity, same texture and CL characteristics, with the pore-filling cement outside the grain. Unfilled microfractures (Fig. 11b) were not connected to the poral network and they were potentially quickly isolated by the calcite mineral growing in the pore space. It is less likely that they formed after cement precipitation,
500 otherwise the cement would have been broken.

7.2 Role of deformation bands on fluid flow and diagenesis

The localized diagenesis observed in form of nodules at Loiano and Bollène provides evidence for the effect of structural heterogeneities, such as DBs, on fluid flow in porous sandstones (Eichhubl et al., 2004, 2009; Balsamo et al., 2012; Philit et al., 2015; Del Sole and Antonellini, 2019; Pizzati et al., 2019; Del Sole et al., 2020). The petrophysical
505 properties (porosity, permeability, capillary entry pressure) of DBs influence fluid flow and localize diagenesis and cement precipitation.

A marked grain-surface roughening and reduction of grain-size, porosity, and pore-size characterize the DBs presented in this work. In *Loiano*, the combined effect of cataclasis and compaction in the DBs causes porosity reduction by one order of magnitude, permeability reduction by three orders of magnitude, and advective velocity reduction by 2 orders of
510 magnitude with respect to the host rock (Del Sole and Antonellini, 2019; Supplement S3). Similarly, DBs in the *Bollène* quarry have lower permeability (up to 3 orders of magnitude) and porosity (up to 50%) (Ballas et al., 2014; Supplement S3)

when compared to the host rock. Cataclastic DBs negatively affect flow tortuosity in reservoirs and produce capillary barriers that severely baffle the flow at the reservoir scale and limit cross flow between host rock compartments (Harper and Mofta, 1985; Edwards et al., 1993; Lewis and Couples, 1993; Antonellini and Aydin, 1994; Leveille et al., 1997; Gibson, 1998; Antonellini et al., 1999, 2014; Sternlof et al., 2004; Rotevatn and Fossen, 2011; Ballas et al., 2012; Medici et al., 2019; Romano et al., 2020). Smaller pores within bands result in higher capillary forces than in the host rock. This may cause higher water saturation within the bands with respect to the host rock (Tueckmantel et al., 2012; Liu and Sun, 2020). Higher degree of flow tortuosity (reduction in pore interconnectivity) and lower porosity and permeability within the bands may increase the fluid retention time regardless of the water-saturation conditions (Antonellini et al., 1999; Sigda and Wilson, 2003; Wilson et al., 2006). Recently, Romano et al. (2020) documented with single and multiphase core flooding experiments that cataclastic bands can strongly influence the fluid velocity field. Other authors (Taylor and Pollard, 2000; Eichhubl et al., 2004) recognized that a slower rate of solute transport relative to the fluid within the bands causes the formation and local perturbation of diagenetic alteration fronts. In light of these considerations and the temporal and spatial relationships between bands and cements obtained from field and microstructural observations, we propose a model for selective cement precipitation associated with DBs. In our model we assume a reservoir in saturated condition (see also Sect. 7.3).

We propose that the presence of the bands in *Loiano* and *Bollène* slowed down the fluid flow. This happens because the bands have lower permeability and transmissibility, a higher degree of tortuosity (i.e. lower pore size) and reduced section area available for flow (i.e. lower porosity) with respect to the host rock (Ballas et al., 2014; Del Sole and Antonellini, 2019; Del Sole et al., 2020; see also Supplement S3). In *Loiano*, the "slow down" effect would be more pronounced when considering the normal-to-DB flow than the parallel-to-DB one given that normal-to-DB permeabilities are lower (1 order of magnitude in average) when compared to parallel-to-DB ones (Del Sole et al., 2020). Cataclasis has competing effects on advective flow velocity; it causes (i) an increase of flow velocity linked to the porosity reduction and (ii) a decrease of the hydraulic conductivity (if the hydraulic gradient does not change). The decrease of hydraulic conductivity (3 orders of magnitude; Del Sole and Antonellini, 2019) dominates over the flow velocity increase caused by porosity reduction (1 order of magnitude; Del Sole and Antonellini, 2019). As a result, there is a net decrease in advective flow velocity in the DBs. A reduction in flow velocity (i.e. slower flow path in the DB with respect to the host rock) might increase the residence time of the fluid migrating through the reactive material (see next paragraph), enabling precipitation to take place (Bott, 1995; Walker and Sheikholeslami, 2003). This "slow down", alone, could represent one of the first trigger to promote preferential cement precipitation within the band or in its proximity as observed in the field.

A second mechanism responsible for cement nucleation in association with DBs would be the presence of highly reactive crushed and pervasive fractured siliciclastic grains within the cataclastic DBs (e.g. Lander et al., 2009; Williams et al., 2015). The comminuted material of the DBs owns a large amount of reactive surface area (nucleation spots) and very tiny pores spaces among the crushed grains. With these conditions, cement precipitation requires less free energy to occur (Wollast, 1971; Berner, 1980) whereas greater cement abundances (e.g. Walderhaug, 2000) and faster rates of cement

emplacement (Lander et al., 2008; Williams et al., 2015) are promoted. This mechanism has already been proposed to explain the presence of cement within the bands pore space and contrast in the degree of cementation between the bands and the surrounding rock (Antonellini et al., 1994; Knipe et al., 1997; Fisher and Knipe, 1998; Milliken et al., 2005; Philit et al., 2015; Del Sole and Antonellini, 2019; Pizzati et al., 2019). This mechanism may be relevant for *Loiano* where the calcite cement fills small pore spaces among fresh quartz and feldspar surfaces created during fracturing. This process can explain why in most cases DBs are more cemented than the surrounding host rock. The low-porosity angular fine-grained cataclastic matrix within the bands offers a lower energy barrier for cement nucleation (Wollast, 1971; Berner, 1980), so that it is not necessary for fluids or brines to reach carbonate saturation for cement precipitation at grain contacts (De Yoreo and Vekilov, 2003). On the contrary, this process was less relevant in the *Bollène quarry* where the bands are not cemented by carbonate and the cementation is localized in compartments between zones of bands rather than within them.

A third mechanism could have worked in conjunction with the presence of more reactive fine-grained comminution products to promote cementation in the DBs in *Loiano*. According to their experiments on analog fault gouge, Whitworth et al. (1999) suggested a membrane behavior for faults in sandstones during cross-fault flow and solute-sieving-aided calcite precipitation. A membrane effect and solute-sieving by faults may locally increase the concentrations of components needed for calcite cementation (e.g. Ca and bicarbonate) and induce precipitation. The DBs could have acted as a semipermeable membrane in baffling chemically reactive flow and favor cement precipitation. This process may explain a higher concentration of cement along the DBs in nodules, and the asymmetric distribution of cement on one side of DBs (upstream side; Figs. 4c, e and 9a, e). An analogous mechanism was proposed by other authors to explain the occurrence of preferred and asymmetric distribution of the authigenic alterations (carbonate and clay cements, Eichhubl, 2001; hematite bleaching, Eichhubl et al., 2004) on the upstream side of DBs in sandstones.

Other factors that may have locally favored (the initiation of) calcite cement precipitation, are the growth of cement on detrital grains (*Loiano*, Fig. 10e; *Bollène*, Fig. 11c) and the presence of broken detrital carbonate clasts (e.g. shell fragments) that act as a "seed" (cement nucleation sites) (e.g. Bjørkum and Walderhaug, 1990). The latter case was observed in *Loiano*, mainly in bedding-parallel nodules (Fig. 9c, d). The mechanisms discussed above explain how and why cement precipitation would occur within the band and in its proximity, as observed on-site. Our field observations confirm the theoretical and flow simulations as well as the analog experiments which demonstrated that DBs can negatively affect the fluid flow in porous sandstones (e.g. Rotevatn and Fossen, 2011; Antonellini et al., 2014; Romano et al., 2020) and enhance cement precipitation (e.g. Lander et al., 2009; Williams et al., 2015).

7.3 Structural diagenesis scenario for carbonate nodules formation

We will integrate the petrographic observations and stable isotopes characterization of cements with the meso-scale spatial organization and the micro-scale textural relationships between nodules and DBs to discuss the geochemical conditions and potential fluid sources that controlled the formation of carbonate nodules in the studied areas.

In *Loiano*, the first calcite cement to precipitate is the intraskeletal and pore-lining cement associated with bioclasts in bedding-parallel nodules (Fig. 9c-d). The cement fabric and textures, circumgranular dogtooth and void-filling drusy mosaic, and the dominant bright-orange CL of calcite associated with bioclasts could suggests a meteoric phreatic environment with reducing conditions (low pO_2) (Longman, 1980; Moore, 1989; Hiatt and Pufhal, 2014; Adams and Diamond, 2017). Drusy calcite spars can result from replacement of aragonite in bioclasts that occur in meteoric environments (Flügel, 2013). The second, more pervasive phase of cementation, consists of the intragranular cement observed in all the nodules. The mosaic of blocky sparite with coarse crystals and homogeneous distribution point to meteoric phreatic conditions (Longman, 1980; Flügel, 2013; Adams and Diamond, 2017). In contrast, the dominant bright cathodoluminescence response suggests an environment with reducing (low pO_2) geochemical conditions. Cement zonation could be triggered by the shifting from more reducing (bright CL) to more oxidizing (dark-CL) conditions and vice versa (Barnaby and Rimstidt, 1989) due to water table fluctuations (Li et al., 2017). The intergranular cement pattern is analogous in DBs-parallel nodules and bedding-parallel nodules meaning they probably formed in a similar meteoric phreatic environment. Phreatic meteoric conditions for the nodules formation point to a shallow diagenesis, and it is consistent with the shallow burial depths estimated for the Loiano Sandstones (see Sect. 7.1).

The negative, depleted $\delta^{13}C$ and $\delta^{18}O$ values found in both types of nodules (Fig. 12a) are consistent with a meteoric environment of precipitation (Nelson and Smith, 1996). DBs-parallel and bedding-parallel nodules show a similar composition for $\delta^{18}O$, however bedding-parallel nodules have more depleted $\delta^{13}C$ values. This might reflect a higher contribution of organic carbon from soil-derived CO_2 (Hudson, 1977), possibly indicating that bedding-parallel nodules formed in shallower conditions with respect to DBs-parallel nodules. Another explanation is that the two types of nodules were formed by different episodes of water income with different (external) environmental conditions. The difference in isotopic composition between these two types of nodules, indeed, suggests different cement precipitation timing and water compositions as proposed by McBride et al. (1995) and Milliken et al. (1998).

Cementation pattern can be used to infer the paleo-fluid flow direction at the time of calcite precipitation (Mozley and Goodwin, 1995; Mozley and Davis, 1996; Cavazza et al., 2009; Eichhubl et al., 2009; Balsamo et al., 2012). Bedding-parallel nodules organization within the local rock sequence supports a phreatic condition for these nodules. Clay horizons are considered sealing features at least at short-time scales, so that the formation of bedding-parallel nodules in sand levels below and/or confined in between clay levels let us infer that fluid circulation was not occurring in the vadose zone. Bedding-parallel nodules, then, could have formed by lateral fluid circulation in saturated conditions (Fig. 13a). The occurrence of preferential cementation in coarser sediments is more macroscopic evidence for cementation in phreatic environment, due to higher saturated permeability and larger solute flux (Mozley and Davis, 1996). DBs-parallel nodules, however, indicate that local fluid circulation was mostly driven by these structural heterogeneities. The different spatial arrangements between DBs and nodules in *Loiano* make the paleo-fluid flow direction reconstruction complex. The asymmetric distribution of cement in some nodules associated with DBs can be also explained by lateral fluid circulation (Fig. 13a), and the accumulation of cement would result on the upstream side of the DBs (Fig. 4c, 9, and 13a). In other cases,

cement is roughly symmetrical with respect to the bands, or it is placed in the zones where conjugate bands intersect (Figs. 4b, 5c, and 13a). The most likely interpretation is that both lateral flow in saturated conditions and "direct" meteoric infiltration from the surface, and percolation through the rock succession, contributed to the formation of nodules in *Loiano* (Fig. 13a).

The calcite source (i.e. diffusive supply of Ca^{2+} and HCO^{3-}) possibly derives from the infiltration of $CaCO_3$-saturated meteoric fluids carrying soil-derived CO_2 (Hudson, 1977; Nelson and Smith, 1996), and/or it is autochthonous deriving from detrital carbonate grains in the sandstone layers or intra-formational deriving from shale beds and calcite-rich clays layers (McBride et al., 1995; Milliken et al., 1998). In both the scenarios calcite precipitates where fluid flow slows down in proximity to zones of DBs (DBs-parallel nodules) and low conductivity layers (bedding-parallel nodules). McBride et al. (1995) suggest that calcite precipitation along faults (DBs) in *Loiano* was induced by the mixing of locally derived formation water with meteoric water introduced along the faults or by a loss (exsolution) of CO_2 along the fault zones. These mechanisms, however, assume that DBs were conductive to fluid flow. This hypothesis disagrees with our measurements of the DBs hydraulic behavior (Del Sole and Antonellini, 2019; Del Sole et al., 2020). More likely, carbonate DBs cementation resulted by CO_2-saturated groundwater (Fig. 13a). We cannot exclude the role of active normal faults in the area (Picotti and Pazzaglia, 2008; Picotti et al., 2009; Fig. 2a), that might have had a control on regional subsurface fluid circulation. These faults could have cut through top/bottom seals and driven fluid migration from top/underneath aquifers (Fig. 13a). Episodic fault activity can also favor (episodic) horizontal fluid migration along layering at the time of faulting, and possibly explains the occurrence of nodules (Fig. 13a) and their different isotopic signature (Fig. 12a). From our observations, we can say that the selective cementation process in the Loiano Sandstones depends on "regional" hydrological factors (e.g. topographic gradient, bedding, faults?) coupled, locally, to the presence of DBs.

In the *Bollène quarry*, the relative timing of DBs formation and cementation in the Turonian Sandstones is complex to unravel. Carbonate cementation occurred in between distinct deformation phases with multiple DBs formation (see Sect. 7.1). The dominant dark cathodoluminescence pattern and homogeneous distributed poikilotopic spar texture suggest an oxidizing (high pO_2) meteoric phreatic environment (Longman, 1980; Moore, 1989; Flügel, 2013; Hiatt and Pufhal, 2014). The zonation is induced by unsteady geochemical conditions, and the bright-orange CL growth sub-zones could be related to stages with more reducing conditions (Barnaby and Rimstidt, 1989; Hiatt and Pufhal, 2014). The invariably negative depleted $\delta^{13}C$ and $\delta^{18}O$ values of nodules in Bollène are consistent with a meteoric environment in a continental setting (Nelson and Smith, 1996). Maximum burial depth of the Turonian sandstone was estimated, through stratigraphic constrains, to be 400 ± 100 meters (Ballas et al., 2013; Soliva et al., 2013). This data supports the shallow conditions for nodules diagenesis in Bollène. The phreatic environment is more probable given that in vadose conditions we should have observed meniscus cements, and because massive calcrete such as observed in the study area generally form in groundwater environment (e.g. Alonso-Zarza, 2003). In the vadose zone, besides, DBs would enhance unsaturated flow relative to the host rock (Sigda et al., 1999; Wilson et al., 2006; Cavailhes et al., 2009; Balsamo et al., 2012).

Field evidence suggest that clusters of low permeability DBs in *Bollène* impeded cross-fault flow since no cement was found in superposition with the DBs. The presence of nodules in between the DBs clusters implicates that the DBs forced the fluid flow and localized the diagenesis in parallel-to-bands compartments. This evidence and the fact that nodules are homogenous along their elongation direction discredit the hypothesis of lateral flow. The cement could have been originated from a (i) downward fluid flow directly from infiltration of meteoric waters, or (ii) an upward flow of basinal fluid (pressurized aquifer) along fractures and faults pathways in the carbonate rocks (Fig. 13b). In both cases, the water flow was potentially driven from the vertical continuity of DBs clusters, that have acted as the propagation features of faults in overlying (i) or underlying (ii) series and aquifers (Fig. 13b). This scenario might explain why the cement is found only in association with the NW-SE DBs. In both cases (i) and (ii), the constituent necessary for the precipitation of cement in nodules (i.e. Ca and bicarbonate) would come from the surrounding carbonates. Above the Turonian sandstones there are several carbonate layers in the Upper Turonian and Santonian interval (Fig. 2c; Ferry, 1997), whereas below there are carbonates belonging to the Jurassic and Cretaceous series (Fig. 2b, c; Debrand-Passard et al., 1984). In the first case (i) continental meteoric waters saturated with meteoric carbon dioxide have dissolved the necessary constituents along their path through the rock succession toward the high-porosity Turonian Sandstones. The water percolation through the soil favored fluids acidification. Similar depleted $\delta^{18}O$ values between nodules and cement from the calcrete level (Fig. 12b) support the (i) hypothesis, and they may have originated from similar surficial cement source from downward water flow in association with variations of bicarbonate concentration and/or pH in the water table. In the second (ii) hypothesis nodule cement resulted from CO_2 exsolution during the upward flow of basinal brine or CO_2-saturated groundwater in a pressurized aquifer.

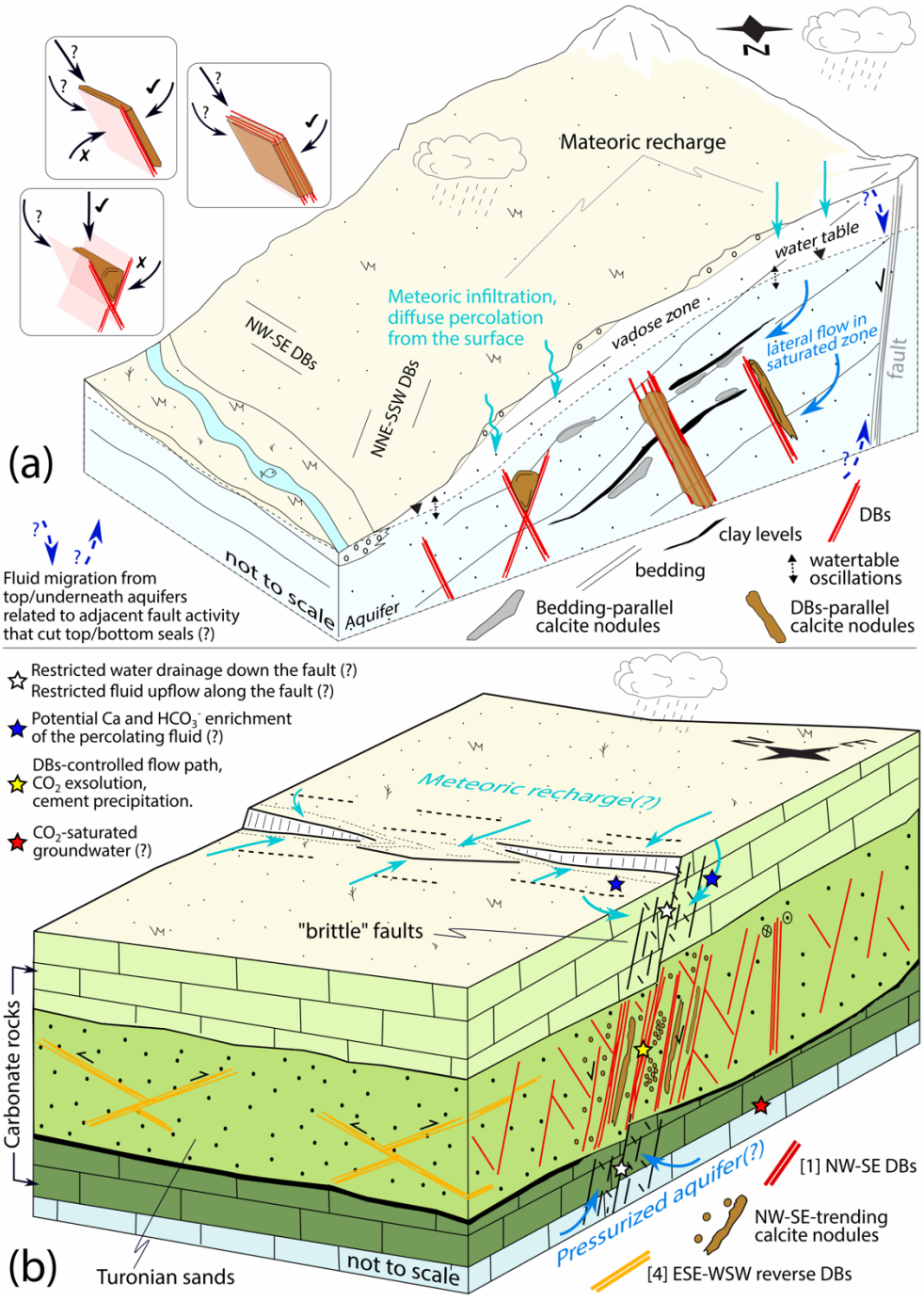

Figure 13. Generalized conceptual model for calcite nodules precipitation in the two study areas: (a) Loiano and (b) Bollène. See text (Sect. 7.3) for details. The inset sketches in (a) show possible paleo-fluid flow direction at the time of calcite precipitation for different "DBs-nodule" configurations.

7.4 Implications for subsurface fluid flow, reservoir characterization, and resources development

Models for calcite cementation are of fundamental importance for predicting sandstone and fault-rock properties such as porosity, permeability, compressibility, and seismic attributes. In Loiano, zone of DBs has acted as fluid flow baffles. First, they slowed the fluid flow and localized cement precipitation, acting as areas of preferential cementation in otherwise excellent porosity sandstones. The resulting diagenetic products enhance porosity and permeability reduction caused by cataclasis, further affecting subsequent fluid circulation. The presence of structural-related cement in the form of concretions i) strengthens the rock volume, ii) degrade porosity and permeability increasing the buffering effect or sealing capacity of zone of DBs, and iii) impart mechanical and petrophysical anisotropy to the host rock (Del Sole et al., 2020). We think that it is important to consider the possibility of concretions to form in association with faults within siliciclastic reservoirs, especially where these structures (DBs) are below seismic resolution (e.g. Del Sole et al., 2020). It is also critical to understand structural diagenesis heterogeneities (SHD) spatial organization, extension, continuity, density, their hydraulic role in terms of fluid flow circulation as well as their mechanical influence on the host rock. This information should be included in a robust reservoir characterization and, in general, it is beneficial during geofluids exploration and energy appraisal, resources development strategies (groundwater, geothermal, hydrocarbon), well production, reservoir simulation modeling, geomechanical evaluation of a drilling site, and other environmental and industrial operations (e.g. waste fluid disposal; groundwater contaminants; geologic CO_2 sequestration; Enhanced Oil Recovery [EOR]). The incorporation of this information into aquifer/reservoir (flow) models requires implicit representation of the SDH network and the upscaling of its (structural and petrophysical) properties (e.g. Fachri et al., 2013; Antonellini et al., 2014). When the cementation is heterogeneous, such as in the examples presented in our work, it could be difficult to model and predict, especially when data are spatially discontinuous (e.g. wells). In these cases, outcrop-based studies allow continuous and more reliable reconstruction of the cement distribution. The characterization of SDH network distribution (e.g. Del Sole et al., 2020) allows to predict where (i.e. location and volumes) and how (i.e. spatial organization) the reservoir compartments are arranged and how the fluid circulation can be affected. The kind of study that we present here might be helpful to extract those statistical parameters necessary to implement reservoir studies that account for heterogeneity in petrophysical properties and their association with seismic/subseismic structural heterogeneities.

8 Conclusions

In this contribution, we present two examples of structural control exerted by deformation bands on fluid flow and diagenesis recorded by calcite nodules strictly associated with deformation bands. The objective of this research was to constrain the role of deformation bands in affecting the flow pattern and in localizing cement precipitation in porous sandstones, as well as to elucidate the mechanisms involved in these processes. The major results of our study can be summarized as follows:

(1) In both study sites, one or more sets of DBs precede and control selective calcite cement precipitation in the form of nodules. The later localization of cementation along these structural features results in a complex and spatially heterogenous cementation pattern (SDH).

(2) Selective cementation of nodules associated with DBs indicates interaction between deformation structures, fluid flow, and chemical processes. The volumetrically significant presence of cement (10-25% of the exposed outcrops volume) indicates that fluid flow and mass transport have been strongly affected by the presence of low permeability DBs.

(3) Three main processes are discussed to explain selective carbonate cementation associated with low permeability DBs. (i) The DBs slow down the advection velocity and promote cement precipitation in the low velocity zone. (ii) Solute-sieving across the DB (membrane effect) promotes Ca and bicarbonate concentration increase on the upstream side. (iii) The high concentration of nucleation sites on the fine-grained comminution products with increased reactive surface area of the pore-grain interface in the DB triggers cement precipitation and fast growth rates. Our hypotheses are supported by field and microstructural observations and petrophysical data.

(4) In *Loiano*, mechanisms (i) through (iii) of bullet (3) likely contributed to selective cement precipitation within the bands and in their proximities, and asymmetric cement distribution with respect to the bands. In *Bollène* no clear superposition among bands and cement was observed and only the first mechanism (i) applies. Here, the clusters of bands acted as hydraulic barriers to cross-flow, thus compartmentalizing the fluid circulation and localizing diagenesis in volumes arranged parallel to the bands.

(5) In both areas, cement texture and cathodoluminescence patterns, and their invariably negative, depleted $\delta^{13}C$ and $\delta^{18}O$ values suggest a shallow meteoric environment for nodules formation.

(6) In a framework of late-stage diagenesis (post-DBs formation) and saturated conditions (meteoric phreatic environment), the processes commonly employed to explain focused fluid flow and preferential cement precipitation associated with DBs, such as “transient dilation” and “capillary suction” (see Sect. 1), appear to be not pertinent. In Bollène and Loiano the DBs buffered and compartmentalized the fluid flow and localized the diagenesis.

(7) Further analyses, such as flow simulations and cement precipitation modeling, are deemed necessary to further explore micro-scale fluid flow and diagenetic mechanisms that drove preferential calcite cement precipitation along DBs in porous sandstones.

(8) DBs control flow pattern and affect how diagenetic heterogeneities are distributed within a porous sandstone. The association of diagenetic cementation with DBs further increases the flow buffering potential of these structural features. It also creates SDH that impart a mechanical and petrophysical anisotropy to the host rock volume and can seriously affect the subsurface fluid circulation in porous sandstones. These features should be considered during reservoir characterization especially where SDH are below seismic resolution.

Data availability. Most of the data produced and used to write the paper are contained in it. More detailed information will be made available on request by contacting the corresponding author.

Author contribution. MA and LDS conceived the paper. LDS collected and processed field and laboratory data, provided their interpretations, drew the figures and wrote the manuscript, and did the revisions. RS and GB contributed to field work in Bollène study site and to cathodoluminescence data interpretation. MA, FB, and GV participated to field work in Loiano study site. All authors actively participated in discussing the results and drawing the conclusions, and critically revised the manuscript.

Competing interest. The authors declare that they have no conflict of interest.

Acknowledgments. LDS kindly acknowledge N. A. Vergara Sassarini for fruitful discussion concerning the interpretation of cathodoluminescence imaging data and M. Pizzati for technical support during sampling for stable isotope analysis. The Laboratoire Géosciences Montpellier at the University of Montpellier is acknowledged for hosting LDS as a visiting PhD student in the period between April and July 2019, during which the cathodoluminescence analysis and the fieldwork in *Bollène quarry* were carried out. The authors wish also to thank P. Iacumin, E. M. Selmo, and A. Di Matteo for stable isotope analysis at the SCVSA Department at the University of Parma. Constructive criticisms and comments by James P. Evans and Geoffrey C. Rawling greatly improved our manuscript. This research is part of a PhD project of the first author. LDS dedicates this work to the loving memory of Antonio Del Sole.

References

Adams, A. and Diamond, L. W.: Early diagenesis driven by widespread meteoric infiltration of a Central European carbonate ramp: A reinterpretation of the Upper Muschelkalk, Sediment. Geol., 362, 37-52, https://doi.org/10.1016/j.sedgeo.2017.10.002, 2017.

Alonso-Zarza, A. M.: Palaeoenvironmental significance of palustrine carbonates and calcretes in the geological record, Earth Sci. Rev., 60(3-4), 261-298, https://doi.org/10.1016/S0012-8252(02)00106-X, 2003.

Antonellini, M. and Aydin, A.: Effect of faulting on fluid flow in porous sandstones: petrophysical properties, AAPG Bull., 78 (3), 355–377, https://doi.org/10.1306/BDFF90AA-1718-11D7-8645000102C1865D, 1994.

Antonellini, M., Aydin, A., and Pollard, D.D.: Microstructure of deformation bands in porous sandstones at Arches National Park, Utah, J. Struct. Geol. 16 (7), 941–959, https://doi.org/10.1016/0191-8141(94)90077-9, 1994.

Antonellini, M., Aydin, A., and Orr, L.: Outcrop-aided characterization of a faulted hydrocarbon reservoir: Arroyo Grande oil field, California, USA, in: Faults and Subsurface Fluid Flow in the Shallow Crust, edited by: Haneberg, W. C., Mozley, P. S., Moore, J. C., and Goodwin, L. B., American Geophysical Union, Washington, DC, 113, 7-26, https://doi.org/10.1029/GM113p0007, 1999.

Antonellini, M., Cilona, A., Tondi, E., Zambrano, M., and Agosta, F.: Fluid flow numerical experiments of faulted porous

carbonates, northwest Sicily (Italy), Mar. Pet. Geol., 55, 186–201, https://doi.org/10.1016/j.marpetgeo.2013.12.003, 2014.

Antonellini, M., Mollema, P.N., and Del Sole, L.: Application of analytical diffusion models to outcrop observations: implications for mass transport by fluid flow through fractures, Water Resour. Res. 53 (7), 5545–5566, https://doi.org/10.1002/2016WR019864, 2017.

Antonellini, M., Del Sole, L., and Mollema, P.N.: Chert nodules in pelagic limestones as paleo-stress indicators: a 3D geomechanical analysis. J. Struct. Geol, 132, 103979, https://doi.org/10.1016/j.jsg.2020.103979, 2020.

Arthaud, F. and Séguret, M.: Les structures pyrénéennes du Languedoc et du Golfe du Lion (Sud de la France). Bull. Soc. Géol. Fr. 23, 51-63, 1981.

Aydin, A.: Small faults formed as deformation bands in sandstones, Pure Appl. Geophys. 116, 913–930, 1978.

Aydin, A.: Fractures, faults, and hydrocarbon entrapment, migration and flow, Mar. Pet. Geol., 17(7), 797-814, https://doi.org/10.1016/S0264-8172(00)00020-9, 2000.

Aydin, A., Borja, R.I. and Eichhubl, P.: Geological and mathematical framework for failure modes in granular rock, J. Struct. Geol. 28 (1), 83–98, https://doi.org/10.1016/j.jsg.2005.07.008, 2006.

Ballas, G., Soliva, R., Sizun, J.P., Benedicto, A., Cavailhes, T., and Raynaud, S.: The importance of the degree of cataclasis in shear bands for fluid flow in porous sand- stone, Provence, France, AAPG Bull., 96 (11), 2167–2186, DOI:10.1306/04051211097, 2012.

Ballas, G., Soliva, R., Sizun, J. P., Fossen, H., Benedicto, A., and Skurtveit, E.: Shear-enhanced compaction bands formed at shallow burial conditions; implications for fluid flow (Provence, France), J. Struct. Geol., 47, 3-15, https://doi.org/10.1016/j.jsg.2012.11.008, 2013.

Ballas, G., Soliva, R., Benedicto, A., and Sizun, J.P.: Control of tectonic setting and large-scale faults on the basin-scale distribution of deformation bands in porous sandstone (Provence, France), Mar. Pet. Geol., 55, 142–159, https://doi.org/10.1016/j.marpetgeo.2013.12.020, 2014.

Ballas, G., Fossen, H., and Soliva, R.: Factors controlling permeability of cataclastic deformation bands and faults in porous sandstone reservoirs, J. Struct. Geol. 76, 1-21, https://doi.org/10.1016/j.jsg.2015.03.013, 2015.

Balsamo F. and Storti F.: Grain size and permeability evolution of soft-sediment extensional sub-seismic and seismic fault zones in high-porosity sediments from the Crotone basin, southern Apennines, Italy, Mar. Pet. Geol., 27, 822-837, https://doi.org/10.1016/j.marpetgeo.2009.10.016, 2010.

Balsamo, F., Storti, F., and Gröcke, D.R.: Fault-related fluid flow history in shallow marine sediments from carbonate concretions, Crotone basin, south Italy, J. Geol. Soc. 169 (5), 613–626, http://dx.doi.org/10.1144/0016-76492011-109, 2012.

Barnaby, R.J. and Rimstidt, J.D.: Redox conditions of calcite cementation interpreted from Mn and Fe contents of authigenic calcites. Geol. Soc. Am. Bull., 101, 795–804, https://doi.org/10.1130/0016-7606(1989)101<0795:RCOCCI>2.3.CO;2, 1989.

Bense, V. F., Gleeson, T., Loveless, S. E., Bour, O., and Scibek, J.: Fault zone hydrogeology, Earth Sci. Rev., 127, 171-192, https://doi.org/10.1016/ j.earscirev.2013.09.008, 2013.

Bernabé, Y., Fryer, D.T., and Hayes, J.A.: The effect of cement on the strength of granular rocks, Geophys. Res. Lett. 19 (14), 1511–1514, https://doi.org/10.1029/92GL01288, 1992.

Berner, R.A.: Early Diagenesis: a Theoretical Approach, Princeton University Press, Princeton, N.J., 1980.

Bjørkum, P.A., and Walderhaug, O.: Geometrical arrangement of calcite cementation within shallow marine sandstones, Earth Sci. Rev. 29 (1–4), 145–161, https://doi.org/10.1016/0012- 8252(90)90033-R, 1990.

Bott, T. R.: *Fouling of heat exchangers*. Elsevier Science B.V. The Netherlands, 1995.

Boutt, D. F., Plourde, K. E., Cook, J., and Goodwin, L. B.: Cementation and the hydromechanical behavior of siliciclastic aquifers and reservoirs, Geofluids, 14(2), 189-199, https://doi.org/10.1111/gfl.12062, 2014.

Busch, B., Hilgers, C., Gronen, L., and Adelmann, D.: Cementation and structural diagenesis of fluvio-aeolian Rotliegend sandstones, northern England, J. Geol. Soc. London, 174(5), 855-868, https://doi.org/10.1144/jgs2016-122, 2017.

Cavailhes, T., Soliva, R., Benedicto, A., Loggia, D., Schultz, R.A., and Wibberley, C.A.J.: Are cataclastic shear bands fluid barriers or capillarity conduits? Insight from the analysis of redox fronts in porous sandstones from Provence, France. In: 2nd EAGE International Conference on Fault and Top Seals: From Pore to Basin Scale, September 21–24, 2009 - Montpellier, France, 3 pp, https://doi.org/10.3997/2214-4609.20147185, 2009.

Cavazza, W., Braga, R., Reinhardt, E. G., Zanotti, C.: Influence of host-rock texture on the morphology of carbonate concretions in a meteoric diagenetic environment, J. Sediment. Res., 79(6), 377-388, https://doi.org/10.2110/jsr.2009.047, 2009.

Champion, C., Choukroune, P., and Clauzon, G.: La déformation post-miocène en Provence occidentale. Geodinamica Acta 13, 67–85, https://doi.org/10.1080/09853111.2000.11105365, 2000.

Cibin, U., Cavazza, W., Fontana, D., Milliken, K.L., and McBride, E.F.: Comparison of composition and texture of calcite-cemented concretions and host sandstones, Northern Apennines, Italy, J. Sediment. Res., 63 (5), 945–954, https://doi.org/10.1306/D4267C4E-2B26-11D7-8648000102C1865D, 1993.

Davis, J. M., Roy, N. D., Mozley, P. S., and Hall, J. S.: The effect of carbonate cementation on permeability heterogeneity in fluvial aquifers: An outcrop analog study, Sediment. Geol., 184(3-4), 267-280, https://doi.org/10.1016/j.sedgeo.2005.11.005, 2006.

De Yoreo, J.J. and Vekilov, P.G.: Principles of crystal nucleation and growth, Rev. Mineral. Geochem. 54 (1), 57–93, https://doi.org/10.2113/0540057, 2003.

Debrand-Passard, S., Courbouleix, S., and Lienhardt, M.J.: Synthèse géologique du Sud- Est de la France: stratigraphie et paléogéographie. In: Bureau de Recherches Géologiques et Minières, Mémoire, vol. 215 (Orléans), 1984.

Del Sole, L. and Antonellini, M.: Microstructural, petrophysical, and mechanical properties of compactive shear bands associated to calcite cement concretions in arkose sandstone, J. Struct. Geol. 126, 51–68, https://doi.org/10.1016/j.jsg.2019.05.007, 2019.

Del Sole, L., Antonellini, M., and Calafato, A.: Characterization of sub-seismic resolution structural diagenetic heterogeneities in porous sandstones: Combining ground-penetrating radar profiles with geomechanical and petrophysical in situ measurements (Northern Apennines, Italy), Mar. Pet. Geol., 117, 104375, https://doi.org/10.1016/j.marpetgeo.2020.104375, 2020.

Dewhurst, D. N. and Jones, R. M.: Influence of physical and diagenetic processes on fault geomechanics and reactivation, Journal of Geochemical Exploration, 78, 153-157, https://doi.org/10.1016/S0375-6742(03)00124-9, 2003.

Dvorkin, J., Mavko, G., and Nur, A.: The effect of cementation on the elastic properties of granular material, Mechanics of Materials, 12(3-4), 207-217, https://doi.org/10.1016/0167-6636(91)90018-U, 1991.

Edwards, H. E., Becker, A. D., and Howell, J. A.: Compartmentalization of an aeolian sandstone by structural heterogeneities: permo-Triassic Hopeman Sandstone, Moray Firth, Scotland, Geol. Soc. Spec. Publ., 73(1), 339-365, https://doi.org/10.1144/GSL.SP.1993.073.01.20, 1993.

Ehrenberg, S. N.: Relationship between diagenesis and reservoir quality in sandstones of the Garn formation, Haltenbanken, mid-Norwegian Continental shelf, AAPG Bull., 74(10), 1538-1558, https://doi.org/10.1306/0C9B2515-1710-11D7-8645000102C1865D, 1990.

Eichhubl, P.: Paleo-Fluid Flow Indicators, Stanford Rock Fracture Project, Vol. 12., pp. 10, https://stacks.stanford.edu/file/druid:jp813ns8076/RFP_2001_Eichhubl.pdf, 2001.

Eichhubl, P., Taylor, W.L., Pollard, D.D., and Aydin, A.: Paleo-fluid flow and deformation in the Aztec Sandstone at the Valley of Fire, Nevada—evidence for the coupling of hydrogeologic, diagenetic, and tectonic processes, Geol. Soc. Am., 116 (9–10), 1120–1136, 2004.

Eichhubl, P., Davatzes, N.C., and Becker, S.P.: Structural and diagenetic control of fluid migration and cementation along the Moab fault, Utah, AAPG Bull., 93 (5), 653–681, https://doi.org/10.1130/0016-7606(1974)85<1515:CATGOF>2.0.CO;2, 2009.

Eichhubl, P., Hooker, J.N., and Laubach, S.E.: Pure and shear-enhanced compaction bands in Aztec Sandstone, J. Struct. Geol. 32 (12), 1873–1886, https://doi.org/10.1016/j.jsg.2010.02.004, 2010.

Fachri, M., Rotevatn, A., and Tveranger, J.: Fluid flow in relay zones revisited: Towards an improved representation of small-scale structural heterogeneities in flow models, Mar. Pet. Geol., 46, 144-164, https://doi.org/10.1016/j.marpetgeo.2013.05.016, 2013.

Faulkner, D. R., Jackson, C. A. L., Lunn, R. J., Schlische, R. W., Shipton, Z. K., Wibberley, C. A. J., and Withjack, M. O.: A review of recent developments concerning the structure, mechanics and fluid flow properties of fault zones, J. Struct. Geol., 32(11), 1557-1575, https://doi.org/10.1016/j.jsg.2010.06.009, 2010.

Ferry, S. (Ed.): Actes des Journées Scientifiques CNRS/ANDRA, Apport des forages ANDRA de Marcoule à la connaissance de la marge crétacée rhodanienne. Etude du Gard Rhodanien/EDP sciences, Bagnols-sur-Cèze, pp. 63-91, 1997.

Fisher, Q. J. and Knipe, R.: Fault sealing processes in siliciclastic sediments, Geol. Soc. Spec. Publ., 147(1), 117-134, https://doi.org/10.1144/GSL.SP.1998.147.01.08, 1998.

Flodin, E., Prasad, M., and Aydin, A.: Petrophysical constraints on deformation styles in Aztec Sandstone, southern Nevada, USA, Pure and Applied Geophysics 160, 1589–1610, https://doi.org/10.1007/s00024-003-2377-1, 2003.

Flügel, E.: Microfacies of carbonate rocks: analysis, interpretation and application, Springer Science & Business Media, 2013.

Fossen, H. and Bale, A.: Deformation and their influence on fluid flow, AAPG Bull., 91, 1685–1700, https://doi.org/10.1306/07300706146, 2007.

Fossen, H., Soliva, R., Ballas, G., Trzaskos, B., Cavalcante, C., and Schultz, R. A.: A review of deformation bands in reservoir sandstones: geometries, mechanisms and distribution, in: Subseismic-Scale Reservoir Deformation, edited by: Ashton, M., Dee, S.J., and Wennberg, O.P., Geol. Soc. Spec. Publ., 459(1), 9-33, https://doi.org/10.1144/SP459.4, 2017.

Fowles, J., and Burley, S.: Textural and permeability characteristics of faulted, high porosity sandstones, Mar. Pet. Geol., 11(5), 608-623, https://doi.org/10.1016/0264-8172(94)90071-X, 1994.

Gibson, R. G.: Physical character and fluid-flow properties of sandstone-derived fault zones, Geol. Soc. Spec. Publ., 127(1), 83-97, https://doi.org/10.1144/GSL.SP.1998.127.01.07, 1998.

Harper, T. and Moftah, I.: Skin effect and completion options in the Ras Budran Reservoir, in: Society of Petroleum Engineers Middle East Oil Technical Conference and Exhibition. SPE, 13708, 211–226, https://doi.org/10.2118/13708-MS, 1985.

Heald, M.T. and Renton, J.J.: Experimental study of sandstone cementation, J. Sediment. Res., 36 (4), 977–991, https://doi.org/10.1306/74D715D7-2B21-11D7-8648000102C1865D, 1966.

Hiatt, E. E. and Pufahl, P. K.: Cathodoluminescence petrography of carbonate rocks: a review of applications for understanding diagenesis, reservoir quality and pore system evolution. Short Course, 45, 75-96, 2014.

Hudson, J.D.: Stable isotopes and limestone lithification, J. Geol. Soc. London, 133, 637–660, https://doi.org/10.1144/gsjgs.133.6.0637, 1977.

Kantorowicz, J.D., Bryant, I.D., and Dawans, J.M.: Controls on the Geometry and Distribution of Carbonate Cements in Jurassic Sandstones: Bridport Sands, Southern England and Viking Group, Troll Field, Norway Geol. Soc. Spec. Publ., 36, 103-118, https://doi.org/10.1144/GSL.SP.1987.036.01.09, 1987.

Knipe, R. J., Fisher, Q. J., Jones, G., Clennell, M. R., Farmer, A. B., Harrison, A., Kidd, B., McAllister, E., Porter, J.R., and White, E. A.: Fault seal analysis: successful methodologies, application and future directions, Norwegian Petroleum Soc. Spec. Publ., 7, 15-38, https://doi.org/10.1016/S0928-8937(97)80004-5, 1997.

La Bruna, V., Lamarche, J., Agosta, F., Rustichelli, A., Giuffrida, A., Salardon, R., and Marié, L.: Structural diagenesis of shallow platform carbonates: Role of early embrittlement on fracture setting and distribution, case study of Monte Alpi (Southern Apennines, Italy), J. Struct. Geol., 131, 103940, https://doi.org/10.1016/j.jsg.2019.103940, 2020.

Labaume, P., and Moretti, I.: Diagenesis-dependence of cataclastic thrust fault zone sealing in sandstones. Example from the Bolivian Sub-Andean Zone, J. Struct. Geol. 23, 1659-1675, https://doi.org/10.1016/S0191-8141(01)00024-4, 2001.

Lander, R. H., Larese, R. E., and Bonnell, L. M.: Toward more accurate quartz cement models: The importance of euhedral versus noneuhedral growth rates, AAPG Bull., 92(11), 1537-1563, https://doi.org/10.1306/07160808037, 2008.

Lander, R.H., Solano-Acosta, W., Thomas, A.R., Reed, R.M., Kacewicz, M., Bonnell, L.M., and Hooker, J.N.: Simulation of fault sealing from quartz cementation within cataclastic deformation zones, in: AAPG Hedberg Conference Basin and Petroleum Systems Modeling: New Horizons in Research and Applications, May 3-7, 2009 - Napa, California, USA, 2 pp, 2009.

Laubach, S. E., Olson, J. E., and Gross, M. R.: Mechanical and fracture stratigraphy, AAPG Bull., 93(11), 1413-1426, https://doi.org/10.1306/07270909094, 2009.

Laubach, S.E., Eichhubl, P., Hilgers, C., and Lander, R.H.: Structural diagenesis, J. Struct. Geol. 32 (12), 1866–1872, https://doi.org/10.1016/j.jsg.2010.10.001, 2010.

Leveille, G. P., Knipe, R., More, C., Ellis, D., Dudley, G., Jones, G., Fisher, Q.J., and Allinson, G.: Compartmentalization of Rotliegendes gas reservoirs by sealing faults, Jupiter Fields area, southern North Sea, Geol. Soc. Spec. Publ., 123(1), 87-104, https://doi.org/10.1144/GSL.SP.1997.123.01.06, 1997.

Lewis, H. and Couples, G. D.: Production evidence for geological heterogeneities in the Anschutz Ranch East field, western U.S.A., in: Characterization of fluvial and eolian reservoirs, edited by: C. P. North and D. J. Prosser, Geol. Soc. Spec. Publ., 73, p. 321–338, https://doi.org/10.1144/GSL.SP.1993.073.01.19, 1993.

Li, Z., Goldstein, R.H., and Franseen, E.K.: Meteoric calcite cementation: diagenetic response to relative fall in sea-level and effect on porosity and permeability, Las Negras area, southeastern Spain, Sediment. Geol., 348, 1–18, http://dx.doi.org/10.1016/j.sedgeo.2016.12.002, 2017.

Liu, Z., and Sun, Y.: Characteristics and formation process of contractional deformation bands in oil-bearing sandstones in the hinge of a fold: A case study of the Youshashan anticline, western Qaidam Basin, China, Journal of Petroleum Science and Engineering, 106994, https://doi.org/10.1016/j.petrol.2020.106994, 2020.

Lommatzsch, M., Exner, U., Gier, S., and Grasemann, B.: Structural and chemical controls of deformation bands on fluid flow: interplay between cataclasis and diagenetic alteration: structural and Chemical Controls of Deformation Bands on Fluid Flow, AAPG Bull., 99 (4), 689–710, DOI: 10.1306/10081413162, 2015.

Longman, M.W.: Carbonate diagenetic textures from nearsurface diagenetic environments, AAPG Bull., 64, 461–487, https://doi.org/10.1306/2F918A63-16CE-11D7-8645000102C1865D, 1980.

Machel, H. G.: Application of cathodoluminescence to carbonate diagenesis, in: Cathodoluminescence in geosciences, edited by: Pagel, M., Barbin, V., Blanc, P., and Ohnenstetter D., Springer, Berlin, Heidelberg, pp. 271-301, DOI:10.1007/978-3-662-04086-7, 2000.

Main, I. G., Kwon, O., Ngwenya, B. T., and Elphick, S. C.: Fault sealing during deformation-band growth in porous sandstone. Geology, 28(12), 1131-1134, https://doi.org/10.1130/0091-7613(2000)28<1131:FSDDGI>2.0.CO;2,

2000.

Manzocchi, T., Ringrose, P. S., and Underhill, J. R.: Flow through fault systems in high-porosity sandstones. Geol. Soc. Spec. Publ., 127(1), 65-82, https://doi.org/10.1144/GSL.SP.1998.127.01.06, 1998.

Marroni, M., Meneghini, F., and Pandolfi, L.: A revised Subduction inception model to explain the late cretaceous, double-vergent orogen in the precollisional Western Tethys: Evidence from the Northern Apennines, Tectonics, 36, 2227–2249. https://doi.org/10.1002/2017TC004627, 2017.

Marshall, D.J.: Cathodoluminescence of geological Materials. Unwin Hyman, Boston, 1988.

McBride, E.F., Milliken, K.L., Cavazza, W., Cibin, U., Fontana, D., Picard, M.D., and Zuffa, G.G.: Heterogeneous distribution of calcite cement at the outcrop scale in tertiary sandstones, northern Apennines, Italy. AAPG Bull., 79 (7), 1044–1063, https://doi.org/10.1306/8D2B21C3-171E-11D7-8645000102C1865D, 1995.

Medici, G., West, L. J., Mountney, N. P., and Welch, M.: Permeability of rock discontinuities and faults in the Triassic Sherwood Sandstone Group (UK): insights for management of fluvio-aeolian aquifers worldwide. Hydrogeology Journal, 27(8), 2835-2855, https://doi.org/10.1007/s10040-019-02035-7, 2019.

Milliken, K.L., McBride, E.F., Cavazza, W., Cibin, U., Fontana, D., Picard, M.D., and Zuffa, G.G.: Geochemical history of calcite precipitation in Tertiary sandstones, northern Apennines, Italy, in: Carbonate cementation in sandstones, edited by: Morad, S., International Association of Sedimentologists Special Publication 26, pp. 213–239, https://doi.org/10.1002/9781444304893.ch10, 1998.

Milliken, K. L., Reed, R. M., and Laubach, S. E.: Quantifying compaction and cementation in deformation bands in porous sandstones, in: Faults, fluid flow, and petroleum traps, edited by: R. Sorkhabi and Y. Tsuji, AAPG Mem., 85, 237–249, DOI:10.1306/1033726M85252, 2005.

Moore, C.H.: Carbonate Diagenesis and Porosity, Elsevier, Amsterdam, 1989.

Morad, S., Al-Ramadan, K., Ketzer, J. M., and De Ros, L. F.: The impact of diagenesis on the heterogeneity of sandstone reservoirs: A review of the role of depositional facies and sequence stratigraphy, AAPG Bull., 94(8), 1267-1309, https://doi.org/10.1306/04211009178, 2010.

Mozley, P. S. and Davis, J. M.: Relationship between oriented calcite concretions and permeability correlation structure in an alluvial aquifer, Sierra Ladrones Formation, New Mexico, J. Sediment. Res., 66(1), 11-16, https://doi.org/10.1306/D4268293-2B26-11D7-8648000102C1865D, 1996.

Mozley, P.S. and Goodwin, L.B.: Patterns of cementation along a Cenozoic normal fault: a record of paleoflow orientations, Geology 23 (6), 539–542, https://doi.org/10.1130/B25618.1, 1995.

Nelson, C.S. and Smith, A.M.: Stable oxygen and carbon isotope compositional fields for skeletal and diagenetic components in New Zealand Cenozoic nontropical carbonate sediments and limestones: a synthesis and review, New Zealand Journal of Geology and Geophysics, 39, 93–107, https://doi.org/10.1080/00288306.1996.9514697, 1996.

Ogilvie, S. R. and Glover, P.W.: The petrophysical properties of deformation bands in relation to their

microstructure, Earth Planet. Sci. Lett., 193(1-2), 129-142, https://doi.org/10.1016/S0012-821X(01)00492-7, 2001.

Papani, L.,: Le arenarie di Loiano nel contesto dell'Appennino settentrionale. Ph.D. thesis. Universita` di Bologna, Bologna, pp. 40, 1998.

Parnell, J., Watt, G. R., Middleton, D., Kelly, J., and Baron, M.: Deformation band control on hydrocarbon migration, J. Sediment. Res., 74(4), 552-560, https://doi.org/10.1306/121703740552, 2004.

Parry, W. T., Chan, M. A., and Beitler, B.: Chemical bleaching indicates episodes of fluid flow in deformation bands in sandstone, AAPG Bull., 88(2), 175-191, https://doi.org/10.1306/09090303034, 2004.

Pei, Y., Paton, D. A., Knipe, R. J., and Wu, K.: A review of fault sealing behaviour and its evaluation in siliciclastic rocks. Earth Sci. Rev., 150, 121-138, http://dx.doi.org/10.1016/j.earscirev.2015.07.011, 2015.

Petrie, E. S., Petrie, R. A., and Evans, J. P.: Identification of reactivation and increased permeability associated with a fault damage zone using a multidisciplinary approach. J. Struct. Geol., 59, 37-49, https://doi.org/10.1016/j.jsg.2013.11.008, 2014.

Philit, S., Soliva, R., Labaume, P., Gout, C., and Wibberley, C.: Relations between shallow cataclastic faulting and cementation in porous sandstones: first insight from a groundwater environmental context. J. Struct. Geol., 81, 89–105, https://doi.org/10.1016/j.jsg.2015.10.001, 2015.

Philit, S., Soliva, R., Castilla, R., Ballas, G., and Taillefer, A.: Clusters of cataclastic deformation bands in porous sandstones. J. Struct. Geol., 114, 235–250, https://doi.org/10.1016/j.jsg.2018.04.013, 2018.

Philit, S., Soliva, R., Ballas, G., Chemenda, A., and Castilla, R.: Fault surface development and fault rock juxtaposition along deformation band clusters in porous sandstones series. AAPG Bull., 103(11), 2731-2756, doi: 10.1306/01211917256, 2019.

Picotti, V. and Pazzaglia, F. J.: A new active tectonic model for the construction of the Northern Apennines mountain front near Bologna (Italy). J. Geophys. Res.: Solid Earth, 113(B8), doi:10.1029/2007JB005307, 2008.

Picotti, V., Ponza, A., and Pazzaglia, F. J.: Topographic expression of active faults in the foothills of the Northern Apennines. Tectonophysics, 474(1-2), 285-294, doi:10.1016/j.tecto.2009.01.009, 2009.

Pizzati, M., Balsamo, F., Storti, F., and Iacumin, P.: Physical and chemical strain-hardening during faulting in poorly lithified sandstone: The role of kinematic stress field and selective cementation. Geol. Soc. Am. Bull., 132 (5-6): 1183–1200, https://doi.org/10.1130/b35296.1, 2019.

Qu, D. and Tveranger, J.: Incorporation of deformation band fault damage zones in reservoir models. AAPG Bull., 100(3), 423-443, DOI:10.1306/12111514166, 2016.

Romano, C. R., Zahasky, C., Garing, C., Minto, J. M., Benson, S. M., Shipton, Z. K., and Lunn, R. J.: Sub-core scale fluid flow behavior in a sandstone with cataclastic deformation bands. Water Resour. Res., DOI: 10.1029/2019WR026715, 2020.

Rotevatn, A. and Fossen, H.: Simulating the effect of subseismic fault tails and process zones in a siliciclastic reservoir

analogue: implications for aquifer support and trap definition. Mar. Pet. Geol., 28, 1648-1662, doi:10.1016/j.marpetgeo.2011.07.005, 2011.

Rotevatn, A., Sandve, T. H., Keilegavlen, E., Kolyukhin, D., and Fossen, H.: Deformation bands and their impact on fluid flow in sandstone reservoirs: the role of natural thickness variations. Geofluids, 13(3), 359-371, https://doi.org/10.1111/gfl.12030, 2013.

Roure, F., Brun, J.P., Colletta, B., and Van den Driessche, J.: Geometry and kinematics of extensional structures in the Alpine Foreland Basin of southeastern France. J. Struct. Geol., 14, 503-519, https://doi.org/10.1016/0191-8141(92)90153-N, 1992.

Saillet, E. and Wibberley, C.A.J.: Evolution of cataclastic faulting in high-porosity sandstone, Bassin du Sud-Est, Provence, France. J. Struct. Geol., 32, 1590-1608, https://doi.org/10.1016/j.jsg.2010.02.007, 2010.

Salvini, F.: Daisy 3: The Structural Data Integrated System Analyzer Software. University of Roma Tre, Rome, available at: http://host.uniroma3.it/progetti/fralab/Downloads/Programs/, 2004.

Sample, J. C., Woods, S., Bender, E., and Loveall, M.: Relationship between deformation bands and petroleum migration in an exhumed reservoir rock, Los Angeles Basin, California, USA. Geofluids, 6(2), 105-112, doi:10.1111/j.1468-8123.2005.00131.x, 2006.

Séranne, M., Benedicto, A., Labaume, P., Truffert, C., and Pascal, G.: Structural style and evolution of the gulf of Lion Oligo-miocene rifting: role of the Pyrenean orogeny. Mar. Pet. Geol. 12 (8), 809-820, https://doi.org/10.1016/0264-8172(95)98849-Z, 1995.

Shipton, Z. K., Evans, J. P., Robeson, K. R., Forster, C. B., and Snelgrove, S.: Structural heterogeneity and permeability in faulted eolian sandstone: Implications for subsurface modeling of faults. AAPG bulletin, 86(5), 863-883, https://doi.org/10.1306/61EEDBC0-173E-11D7-8645000102C1865D, 2002.

Shipton, Z.K., Evans, J.P., and Thompson, L.B.: The geometry and thickness of deformation-band fault core and its influence on sealing characteristics of deformation-band fault zones, in: Faults, fluid flow, and petroleum traps, edited by: R. Sorkhabi and Y. Tsuji, AAPG Mem., 85, 181-195, DOI:10.1306/1033723M853135, 2005.

Sigda, J.M. and Wilson, J.L.: Are faults preferential flow paths through semiarid and arid vadose zones? Water Resour. Res. 39 (8), https://doi.org/10.1029/2002WR001406, 2003.

Sigda, J. M., Goodwin, L. B., Mozley, P. S., and Wilson, J. L.: Permeability alteration in small-displacement faults in poorly lithified sediments: Rio Grande Rift, Central New Mexico, in: Faults and Subsurface Fluid Flow in the Shallow Crust, edited by: Haneberg, W. C., Mozley, P. S., Moore, J. C., and Goodwin, L. B., American Geophysical Union, Washington, DC, 51-68, https://doi.org/10.1029/GM113p0051, 1999.

Soliva, R., Schultz, R.A., Ballas, G., Taboada, A., Wibberley, C., Saillet, E., and Benedicto, A.: A model of strain localization in porous sandstone as a function of tectonic setting, burial and material properties; new insight from Provence (southern France). J. Struct. Geol., 49, 50–63, http://dx.doi.org/10.1016/j.jsg.2012.11.011, 2013.

Soliva, R., Ballas, G., Fossen, H., and Philit, S.: Tectonic regime controls clustering of deformation bands in porous

sandstone. Geology 44 (6), 423–426, doi:10.1130/G37585.1, 2016.

Sternlof, K. R., Chapin, J. R., Pollard, D. D., and Durlofsky, L. J.: Permeability effects of deformation band arrays in sandstone. AAPG Bull., 88(9), 1315-1329, https://doi.org/10.1306/032804, 2004.

Taylor, W. L. and Pollard, D. D.: Estimation of in situ permeability of deformation bands in porous sandstone, Valley of Fire, Nevada. Water Resour. Res. 36(9), 2595-2606, https://doi.org/10.1029/2000WR900120, 2000.

Tenthorey, E., Scholz, C.H., Aharonov, E., and Leger, A.: Precipitation sealing and diagenesis 1. Experimental results. J. Geophys. Res.: Solid Earth 103 (B10), 23951-23967, https://doi.org/10.1029/98JB02229, 1998.

Torabi, A., and Fossen, H.: Spatial variation of microstructure and petrophysical properties along deformation bands in reservoir sandstones. AAPG Bull., 93(7), 919-938, https://doi.org/10.1306/03270908161, 2009.

Tueckmantel, C., Fisher, Q. J., Grattoni, C. A., and Aplin, A. C.: Single-and two-phase fluid flow properties of cataclastic fault rocks in porous sandstone. Mar. Pet. Geol., 29(1), 129-142, doi:10.1016/j.marpetgeo.2011.07.009, 2012.

Vai, G. B., Martini, I. P. (Eds.): Anatomy of an orogen: The Apennines and Adjacent Mediterranean Basins, p. 637, Dordrecht, Netherlands, Kluwer Academic Publishers, 2001.

Walderhaug, O.: Modeling quartz cementation and porosity in middle Jurassic Brent Group sandstones of the Kvitebjørn field, Northern North Sea, AAPG Bull., 84, 1325-1339, 2000.

Walker, P. and Sheikholeslami, R.: Assessment of the effect of velocity and residence time in CaSO4 precipitating flow reaction. Chemical engineering science, 58(16), 3807-3816, https://doi.org/10.1016/S0009-2509(03)00268-9, 2003.

Whitworth, T. M., Haneberg, W. C., Mozley, P. S., and Goodwin, L. B.: Solute-sieving-induced calcite precipitation on pulverized quartz sand: experimental results and implications for the membrane behavior of fault gouge, in: Faults and Subsurface Fluid Flow in the Shallow Crust, edited by: Haneberg, W. C., Mozley, P. S., Moore, J. C., and Goodwin, L. B., American Geophysical Union, Washington, DC, 149-158, https://doi.org/10.1029/GM113p0149, 1999.

Wibberley, C.A.J., Petit, J.-P., and Rives, T.: The mechanics of fault distribution and localization in high-porosity sands, Provence, France, Geol. Soc. Spec. Publ., 289, 19-46, DOI: 10.1144/SP289.3, 2007.

Wilkins, S. J., Davies, R. K., and Naruk, S. J.: Subsurface observations of deformation bands and their impact on hydrocarbon production within the Holstein Field, Gulf of Mexico, USA, Geol. Soc. Spec. Publ., 496, https://doi.org/10.1144/SP496-2018-139, 2019.

Williams, R.T., Farver, J.R., Onasch, C.M., and Winslow, D.F.: An experimental investigation of the role of microfracture surfaces in controlling quartz precipitation rate: applications to fault zone diagenesis. J. Struct. Geol., 74, 24-30, https://doi.org/10.1016/j.jsg.2015.02.011, 2015.

Williams, R. T., Goodwin, L. B., and Mozley, P. S.: Diagenetic controls on the evolution of fault-zone architecture and permeability structure: Implications for episodicity of fault-zone fluid transport in extensional basins. Geol. Soc. Am. Bull., 129(3-4), 464-478, https://doi.org/10.1130/B31443.1, 2017.

Wilson, J.E., Goodwin, L.B., and Lewis, C.: Diagenesis of deformation band faults: record and mechanical consequences of vadose zone flow and transport in the Bandelier Tuff, Los Alamos, New Mexico. J. Geophys. Res.: Solid Earth 111 (B9), doi:10.1029/2005JB003892, 2006.

Wollast, R.: Kinetic aspects of the nucleation and growth of calcite from aqueous solutions, in: Carbonate Cements, edited by: Bricker, O.P., Mackenzie, F.T., J. Hopkins Press, 79, 264–273, 1971.